Hydrogen storage in metal–organic frameworks†

Leslie J. Murray, Mircea Dincă and Jeffrey R. Long*

Received 9th December 2008
First published as an Advance Article on the web 25th March 2009
DOI: 10.1039/b802256a

New materials capable of storing hydrogen at high gravimetric and volumetric densities are required if hydrogen is to be widely employed as a clean alternative to hydrocarbon fuels in cars and other mobile applications. With exceptionally high surface areas and chemically-tunable structures, microporous metal–organic frameworks have recently emerged as some of the most promising candidate materials. In this *critical review* we provide an overview of the current status of hydrogen storage within such compounds. Particular emphasis is given to the relationships between structural features and the enthalpy of hydrogen adsorption, spectroscopic methods for probing framework–H_2 interactions, and strategies for improving storage capacity (188 references).

Introduction

In 2005, the daily global consumption of petroleum exceeded 83 million barrels resulting in the release of almost 11 billion metric tonnes of carbon dioxide into the atmosphere.[1] Consumption is expected to increase steadily over the next 50 years, driven in part by higher demands in developing nations. Amid concerns that the escalating atmospheric level of carbon dioxide will irreparably damage the global ecosystem, research into carbon-neutral replacements for fossil fuels is expanding. An alternative fuel for automotive transportation is of particular interest and would have a substantial impact on carbon emissions, with more than 132 million vehicles in the United States alone.[2]

Battery and fuel-cell technologies are strong candidates to replace gasoline and diesel engines. In particular, hydrogen is an attractive energy carrier because it is carbon-free, abundantly available from water, and has an exceptional mass energy density.[3] Unfortunately, hydrogen is an extremely volatile gas under ambient conditions, resulting in a volumetric energy density that is much too low for practical applications. For on-board use, hydrogen must be compressed to very high pressures or stored cryogenically, both of which cost energy and substantially increase vehicle weight. The goal therefore is to design low-cost, light-weight materials that can reversibly and rapidly store hydrogen near ambient conditions at a density equal to or greater than liquid hydrogen. The US Department of Energy 2010 targets for a hydrogen storage system are: a capacity of 45 g H_2 per L, a refuelling time of 10 min or less, a lifetime of 1000 refuelling cycles, and an ability to operate within the temperature range −30 to 50 °C.[4,5] It is important to note that these targets are for the entire storage system, such that the performance of a storage material must be even higher in order to account for the storage container and, if necessary, temperature regulating apparatus.

Hydrogen binds to surfaces by weak dispersive interactions (physisorption) or through stronger chemical associations

Department of Chemistry, University of California, Berkeley, CA, 94720-1460, USA. E-mail: jrlong@berkeley.edu; Fax: +1 510 643 3546; Tel: +1 510 642 0860
† Part of the metal–organic frameworks themed issue.

Leslie J. Murray

Leslie J. Murray (born 1980, Trinidad & Tobago) obtained BA degrees in Chemistry and Biology from Swarthmore College in 2002. He received a PhD in Inorganic Chemistry in 2007 under the supervision of Prof. Stephen J. Lippard at MIT, where he studied component interactions and dioxygen activation in bacterial multicomponent monooxygenases. Currently, he is a postdoctoral associate in Jeffrey R. Long's research group at UC Berkeley and focuses on the design and synthesis of metal–organic frameworks.

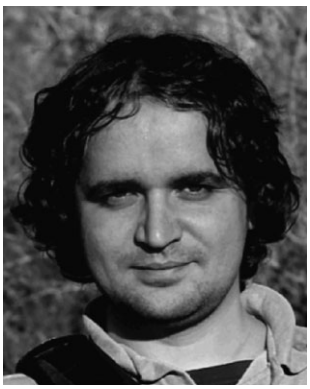

Mircea Dincă

Mircea Dincă (born 1980, Romania) obtained his BA degree in Chemistry from Princeton University in 2003. He then joined Prof. Jeffrey R. Long's group at UC Berkeley and worked in the area of microporous metal–organic frameworks, receiving his PhD degree in 2008. Currently, he is a postdoctoral associate with Prof. Daniel G. Nocera at MIT.

(chemisorption). Physisorption correlates with surface area, with greater gas uptake favored by higher surface area. Thus, materials with large surface areas and low densities, such as metal–organic frameworks and certain activated carbons, are attractive for hydrogen storage applications. In the temperature regime desired for automotive applications, however, dispersive forces cannot facilitate substantial hydrogen uptake. The modular nature of metal–organic frameworks allows for the facile, ordered incorporation of new functionalities to enhance the hydrogen storage properties. Here, we review the current state of hydrogen storage in metal–organic frameworks, focusing on strategies for improving the storage capacity of these compounds. The design of new frameworks depends on a detailed chemical understanding of the interaction of hydrogen at sites within the structure. We therefore also discuss briefly some spectroscopic tools that are available to interrogate hydrogen binding in these systems.

H_2 adsorption in metal–organic frameworks

Excess *versus* total uptake

Most articles dealing with hydrogen storage in metal–organic frameworks report the H_2 uptake capacity at a pressure of *ca.* 1 bar, where excess and total adsorption values are nearly identical. However, since pressures of up to 100 bar are deemed safe for automotive applications, measurements at higher pressures, where these two quantities can differ considerably, have become common. Excess adsorption refers to the amount of H_2 taken up beyond what would be contained, under identical conditions, within a free volume equivalent to the total pore volume of the sample. Thus, this quantity approximates the amount of H_2 adsorbed on the surfaces within the material. Since the efficiency of packing and compressing gas molecules within the confines of the pores of a microporous solid is less than that achieved in a free volume, the excess adsorption will reach a maximum at some pressure (typically 20–40 bar) and then decrease. Despite the decrease, measurements at pressures above the maximum in excess adsorption are of value for assessing the compressibility of H_2 within the material and evaluating the total uptake.

Jeffrey R. Long

Jeffrey R. Long was born in Rolla, Missouri (USA), in 1969. He received a Bachelor's Degree in Chemistry from Cornell University in 1991 and a PhD in Chemistry from Harvard University in 1995. Following postdoctoral work at Harvard and the University of California, Berkeley, he joined the faculty in Chemistry at Berkeley in 1997. His research involves the synthesis of new inorganic clusters and solids with emphasis on magnetic and microporous materials.

The total uptake, sometimes referred to as the absolute uptake, corresponds to the amount of hydrogen contained within the boundaries formed by the faces of the metal–organic framework crystals. This quantity therefore includes both surface-adsorbed H_2 and the H_2 gas compressed within the framework pores. To calculate the total uptake from the excess adsorption, it is necessary to know precisely the density of the framework skeleton or the empty volume of the adsorbent, as typically measured using helium gas. Importantly, knowledge of the total uptake enables determination of the volumetric storage density within the compound, which is one of the main considerations in selecting a hydrogen storage material. It is important to note, however, that this fundamental property of the material does not take into account the efficiency of packing the crystals together in a container, as must be considered in determining the overall density for a storage system.

When calculating the H_2 uptake—either excess or total—in units of wt%, it is important to recognize that it is equal to (mass H_2)/(mass sample + mass H_2). Unfortunately, some researchers neglect the second term in the denominator, leading to complications in comparing uptake capacities for different materials.

Design principles for an optimal H_2 adsorbent

There have been numerous computational studies that attempt to model H_2 adsorption data in metal–organic frameworks.[6–17] In particular, $Zn_4O(BDC)_3$ (BDC^{2-} = 1,4-benzenedicarboxylate; see Fig. 1) and its isoreticulated congeners have received much attention from theorists. In most cases, computed isotherms and binding energy values agree reasonably well with the experimental results, although

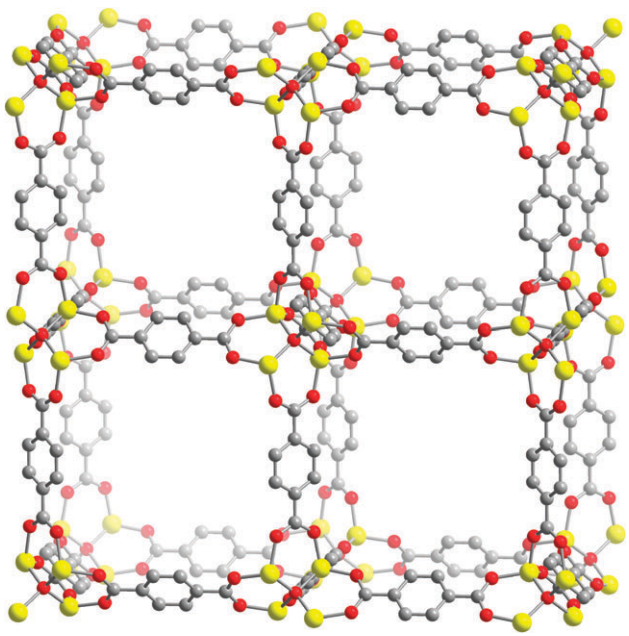

Fig. 1 A portion of the crystal structure of $Zn_4O(BDC)_3$ (MOF-5).[65] Yellow, gray, and red spheres represent Zn, C, and O atoms, respectively; H atoms are omitted for clarity. The three-dimensional structure gives rise to square openings, which are either 13.8 Å or 9.2 Å wide depending on the orientation of the aromatic rings.

one should be careful to employ an accurate intermolecular H_2 potential energy function[18] and to ensure that the comparison data are for an authentic sample.[19] These studies indicate the presence of just van der Waals-type interactions between H_2 and most frameworks, consistent with the approximate correlation of H_2 uptake at 77 K with surface area and the very low storage capacities observed at 298 K. Indeed, with just two electrons, H_2 forms extremely weak van der Waals bonds, resulting in isosteric heats of adsorption that are typically in the range 4–7 kJ mol^{-1}.

Partial charges, either positive or negative, on the metal–organic framework surface can provide a means of strengthening the binding of H_2 through dipole–induced dipole interactions.[6,20] Only a few computational studies have dealt with frameworks exhibiting such heterogeneous surface potentials. These have focused mainly on the chief experimental strategy adopted, that of utilizing frameworks with exposed metal cation sites on the surface. An added complication in performing calculations on frameworks bearing open transition metal coordination sites stems from the fact that these metals sometimes have open-shell electron configurations, for which assignment of the spin state can be difficult. For instance, the relatively strong metal–H_2 interactions within $Mn_3[(Mn_4Cl)_3(BTT)_8]_2$ (H_3BTT = benzene-1,3,5-tris(1*H*-tetrazole)), which exhibits an isosteric heat of adsorption of 10.1 kJ mol^{-1} at zero coverage,[21] have been attributed variously to a spin-state change upon binding[22] or to a classical Coulombic attraction.[23] Understanding metal–H_2 interactions of this type is instrumental to the design of improved storage materials, and the development of computational approaches that can reliably handle interactions with open-shell metal ions would present an important step forward.

Clearly, increasing the H_2 binding energy within metal–organic frameworks is the most important challenge for creating hydrogen adsorbents that operate at 298 K. Recent work has addressed this issue and predicted optimal parameters for hydrogen storage in microporous materials. First, Langmuir isotherms were employed to derive equations that allow the calculation of an optimal adsorption enthalpy, ΔH_{opt}, for a given adsorption temperature.[24] According to this model, which can be reduced to the empirical equation $-\Delta H_{opt}/RT = 6.1$, a microporous adsorbent operating between 1.5 and 100 bar at 298 K would ideally have an adsorption enthalpy of 13.6 kJ mol^{-1} over the entire H_2 uptake curve. Similarly, the model allows one to calculate the optimal operating temperature for an adsorbent with a given enthalpy of adsorption. For instance, it predicts that a typical metal–organic framework with an average adsorption enthalpy of 6 kJ mol^{-1} would function optimally at a temperature of 131 K.

The aforementioned model has recently been adjusted through introduction of an entropy–enthalpy correlation term.[25] Whereas ΔS_{ads} had previously been assumed to be constant and equal to $-8R$, the new model argues that Langmuir adsorption is in fact governed by a positive correlation between entropy and enthalpy. Taking this empirical correlation into account suggests that a material operating between 1.5 and 30 bar at 298 K requires a ΔH_{opt} of 22–25 kJ mol^{-1}, which is significantly higher than that obtained with the previous model. Thus, for pressures ranging up to 100 bar, one would like to create new metal–organic frameworks featuring surfaces with a ΔH_{opt} of *ca.* 20 kJ mol^{-1}, representing an enhancement by a factor of 3 or 4 over simple physisorption.

As expected, in a microporous material where physisorption and weak van der Waals forces dominate the adsorption picture, the storage density is also greatly dependent on the size of the pore. Calculations on idealized homogeneous materials, such as graphitic carbons and carbon nanotubes, predict that microporous materials with 7 Å-wide pores will exhibit maximal H_2 uptake at room temperature. In effect, a 7 Å-wide slit-shaped pore maximizes the van der Waals potential by allowing exactly one layer of H_2 molecules to adsorb on opposing surfaces, with no space left in between. Notably, at 77 K a layer sandwiched in between these two opposing surface monolayers becomes favorable, and the ideal pore size for maximum volumetric H_2 uptake at 100 bar is predicted to be 10 Å, regardless of whether a slit shape or cylindrical pore shape is considered.[26]

Finally, an ideal hydrogen storage material would be stable to any potential impurities that might commonly be present in H_2 gas (*e.g.*, H_2S, carbon–sulfur compounds, CO, CO_2, N_2, H_2O, and hydrocarbons), and to accidental exposure to the atmosphere. Indeed, metal–organic frameworks exhibiting some of the best performance characteristics, such as $Zn_4O(BDC)_3$ and $Mn_3[(Mn_4Cl)_3(BTT)_8]_2$, are known to decompose in air,[19,21,27,28] which would need to be accounted for in the design of a storage system. However, by producing frameworks featuring strong metal–ligand bonds, as occurs for example in metal–imidazolate,[29–31] –triazolate,[32–36] and –pyrazolate[37] frameworks, materials exhibiting improved chemical stability can be obtained.

Methods for increasing the H_2 adsorption enthalpy

Exposed metal sites

Perhaps the most effective means of increasing the H_2 adsorption enthalpy in metal–organic frameworks is through introduction of open metal coordination sites on the surfaces. It is well known that H_2 can bind to metals in molecular systems, where metal–H_2 bond dissociation energies can reach as high as 80–90 kJ mol^{-1}, as observed for $(C_5H_5)V(CO)_3(H_2)$ and $Mo(CO)_5(H_2)$.[38] These values are clearly too large for our purposes, and would result in both a tremendous release of heat upon loading with H_2 and a requirement for significant heat input to liberate the bound H_2 when needed. To achieve the desired binding energy of *ca.* 20 kJ mol^{-1}, we most likely need to avoid the favorable orbital interactions that lead to such strong metal–H_2 bonds and move into the regime of simple charge-induced dipole interactions. This situation is exemplified by the interaction between the Li^+ cation and H_2 in the gas phase, which has been measured, albeit with a large potential error, to have a binding energy of 27 kJ mol^{-1}.[39] Unfortunately, when Li^+ is placed on a surface within a porous framework much of its charge is quenched, leading to significantly weaker H_2 binding. Indeed, the highest

isosteric heat of H_2 adsorption yet observed for such a system is just 7.9 kJ mol^{-1} in $Li_2Zn_3[Fe(CN)_6]_2{\cdot}2H_2O$.[40] To counter this effect, a more highly-charged metal cation, such as Mg^{2+}, M^{2+} (M = transition metal), or even Al^{3+}, may be required.

The challenge is then to develop synthetic methods for generating high concentrations of exposed metal ions on the surfaces within metal–organic frameworks. These methods, together with the properties of the resulting materials, have been reviewed in detail recently,[41] and will therefore receive only brief attention here. The primary method utilized thus far involves thermally-assisted evacuation of solvent molecules bound to metals serving as framework nodes, as for example employed in exposing Cu^{2+} coordination sites within $Cu_3(BTC)_2$ (BTC^{3-} = 1,3,5-benzenetricarboxylate)[27,42] and Mn^{2+} coordination sites within $Mn_3[(Mn_4Cl)_3(BTT)_8]_2$.[21] Here, one is generally fighting against framework collapse, making it sometimes beneficial to exchange the bound solvent molecules for more volatile species, such as methanol. Alternatively, photolysis can sometimes be used to facilitate substitution of a terminal ligand for H_2, as demonstrated recently for $Zn_4O[(BDC)Cr(CO)_3]_3$;[43] however, it is important to recognize the poor efficiency of photolyzing solids. For rare cases of anionic frameworks, exchange of the guest metal cation can affect hydrogen uptake.[28,40,44] Finally, the use of reactive bridging ligands in a framework can enable metalation, as demonstrated with the lithiation of $Zn_2(NDC)_2(diPyNI)$ (NDC^{2-} = 2,6-naphthalene dicarboxylate; diPyNI = *N*,*N*′-di(4-pyridyl)-1,4,5,8-naphthalenetetracarboxydiimide).[45]

Catenation/interpenetration

Very large pores within a metal–organic framework are ultimately detrimental to hydrogen storage, because H_2 molecules near the center of the pore are unlikely to experience any attraction from the potential surface of the pore walls. Accordingly, as will be discussed later, such low-density framework solids will tend to have low volumetric H_2 uptake capacities. Indeed, it is clear that a large micropore volume composed of small voids is more desirable for an efficient storage material.[46] Such a material would adsorb H_2 more strongly, but would still exhibit a high surface area, which has been shown to correlate almost linearly with the overall H_2 uptake for homogeneous, physisorption-based systems.[47]

One could conceivably reduce the number of large voids in a given structure *via* framework interpenetration. Synthetically, however, it is extremely difficult to control interpenetration, and only one example exists wherein catenated and non-catenated forms of the same framework were directly compared for H_2 storage. The catenated version of $Cu_3(tatb)_2$ ($tatb^{3-}$ = 4,4′,4″-*s*-triazine-2,4,6-triyltribenzoate) was found to adsorb 1.9 wt% of H_2 at 1 bar and 77 K,[48] an almost 0.6 wt% improvement over the non-catenated form of the compound.[49] It is unclear whether this improvement can be generalized to other frameworks, or whether the difference between the two isomers would be retained at increased pressure. In principle, one should expect that the surface area for a catenated framework will be reduced relative to its uncatenated analogue, owing to the framework–framework interactions that should arise upon desolvation. In practice, however, catenation can sometimes lend a material enhanced thermal stability, reducing the degree of framework collapse during desolvation.[50] Along these lines, it has been argued recently that catenation is detrimental for the overall uptake.[9] Calculations suggest that the amount of H_2 adsorbed correlates with the heat of adsorption only at low loadings, and that surface area and total free volume become more important at intermediate and high loadings, respectively. It has been argued that the increase in binding energy associated with catenation will not offset the loss of free volume, which negatively affects the total H_2 uptake in a given material.

Spillover

Hydrogen spillover is a well-established phenomenon in surface science, involving the dissociation of H_2 into $H^{\bullet}$ on a metal surface and subsequent migration of these atoms onto materials such as alumina.[51–56] This reaction is reversible, with hydrogen atoms spontaneously recombining to afford the molecular gas. Spillover from a nearby metal site and migration of those hydrogen atoms into the pores of frameworks could enhance the hydrogen storage capacity, provided that no irreversible hydrogenation chemistry occurs and the adsorbate–framework interaction and packing density of $H^{\bullet}$ are greater than that of H_2.[57,58]

To investigate this phenomenon in porous solids, tests were performed on mechanically-formed mixtures of a Pt/C catalyst, consisting of 0.05 g of 20 wt% Pt nanoparticles on activated carbon, with $(C_3H_2BO)_6{\cdot}(C_9H_{12})$ (COF-1), Cu_3BTC_2, $Zn_4O(NDC)_3$, $Zn_4O(BDC)_3$, $Zn_4O(BTB)_2$, Al(OH)(BDC), and $Cr_3OF(BDC)_3$.[59–64] The hydrogen uptake capacities at 298 K and 100 bar were determined for these mixtures, and found to increase by at least two-fold relative to the unmodified framework. Notably, the improved performance of the mixture exceeded the sum of the storage capacities of the individual components, implying that the Pt/C catalyst enhanced the storage properties of the frameworks. It should be noted, however, that mechanical grinding alone does not necessarily afford a good pathway for spillover to occur between the Pt nanocrystals and the framework surface. Addition of a small amount of sucrose, followed by a thermal treatment, which first melts then decomposes the sucrose, generally led to enhanced H_2 uptake, presumably owing to an improved $H^{\bullet}$ migration path. Powder X-ray diffraction patterns of the samples before and after this "bridging" protocol demonstrate that the crystallinity of the metal–organic framework is retained.[61,64] Increases of three-fold or greater have been observed in the hydrogen storage capacity at room temperature relative to the unmodified framework. The bridged materials can show reversible adsorption/desorption through two or sometimes more cycles, but long-term recyclability at high capacity has not yet been demonstrated. In addition to issues with reproducibility and recyclability, the desorption process can be slow, in some cases requiring evacuation for 12 h prior to the second adsorption measurement.

While spillover research has generated some of the most encouraging recent results for room-temperature hydrogen storage, many fundamental questions remain to be addressed.

Understanding the precise form in which hydrogen is stored in these systems may provide the key to improving desorption kinetics and recyclability. If the storage mechanism does in fact involve spillover, then synthetic chemistry can perhaps supply materials in which well-defined metal nanocrystals are directly integrated within metal–organic frameworks. The possibilities of achieving a spillover effect with less-expensive metals, such as nickel, and smaller metal clusters or even individual metal centers also remain to be explored.

Metal–organic frameworks exhibiting a high H_2 uptake

One of the first metal–organic frameworks investigated for hydrogen storage was the cubic carboxylate-based framework $Zn_4O(BDC)_3$ (see Fig. 1).[65] This compound has been widely studied since, and turns out to be the best cryogenic storage material currently known. Early measurements performed at 77 K resulted in an excess gravimetric uptake of 1.3 wt% at 1 bar[66] and 5.1 wt% at 50 bar.[67] Interestingly, the gas storage properties obtained for $Zn_4O(BDC)_3$ were found to depend very much on the methods utilized in its preparation and activation, with Langmuir surface areas ranging between 1010 and 4400 $m^2\ g^{-1}$ and H_2 uptake capacity varying accordingly.[19,31,65–74] The variation can be attributed to incomplete evacuation of the pores and/or partial decomposition of the framework upon exposure to air.[19,75] With complete activation and protection of the sample from air and water, $Zn_4O(BDC)_3$ was observed to exhibit a record excess H_2 uptake of 7.1 wt% at 77 K and 40 bar (see Fig. 2).[19] At 100 bar, a total uptake of 10.0 wt% is attained, corresponding to a record volumetric storage density of 66 g L^{-1}. Remarkably, this value is near the density of 71 g L^{-1} observed for liquid hydrogen at 20.4 K and 1 bar.[79] In addition, it was demonstrated that hydrogen can be loaded into a cold sample of the compound within 2 min, and can be completely desorbed and re-adsorbed for at least 24 cycles without loss of capacity.[19]

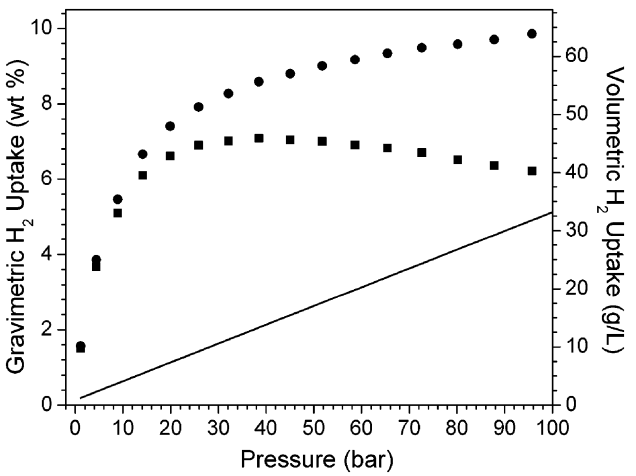

Fig. 2 Excess (squares) and total (circles) hydrogen uptake for $Zn_4O(BDC)$ at 77 K.[19] The solid line represents the density of compressed hydrogen over the given pressure range at this temperature.

Inspired by the performance of compounds such as $Zn_4O(BDC)_3$, researchers have thus far reported hydrogen storage data for over 150 other microporous metal–organic frameworks (see Table 1).[3,77] However, most efforts to date have focused on attaining a high gravimetric uptake, which, importantly, can be at direct odds with achieving a high volumetric storage density. This is because materials with a very high surface area also tend to exhibit an increased micropore volume and, consequently, an inherently low bulk density. Consider, for example, the case of $Zn_4O(BTB)_2$ (BTB^{3-} = 1,3,5-benzenetribenzoate), wherein tetrahedral $[Zn_4O]^{6+}$ units are linked *via* a large, triangular tricarboxylate ligand (see Fig. 3). At 77 K, this compound exhibits a maximal excess H_2 uptake of 76 mg H_2 per 1076 mg compound + H_2 = 7.1 wt%,[69,78] matching that of $Zn_4O(BDC)_3$. However, owing to its significantly larger pores, much of the H_2 stored within $Zn_4O(BTB)_2$ is simply compressed within the empty volume, rather than adsorbed on the framework surface. This leads to a higher total gravimetric uptake, reaching 11.4 wt% at 78 bar and 77 K, but, correspondingly, a *lower* volumetric storage

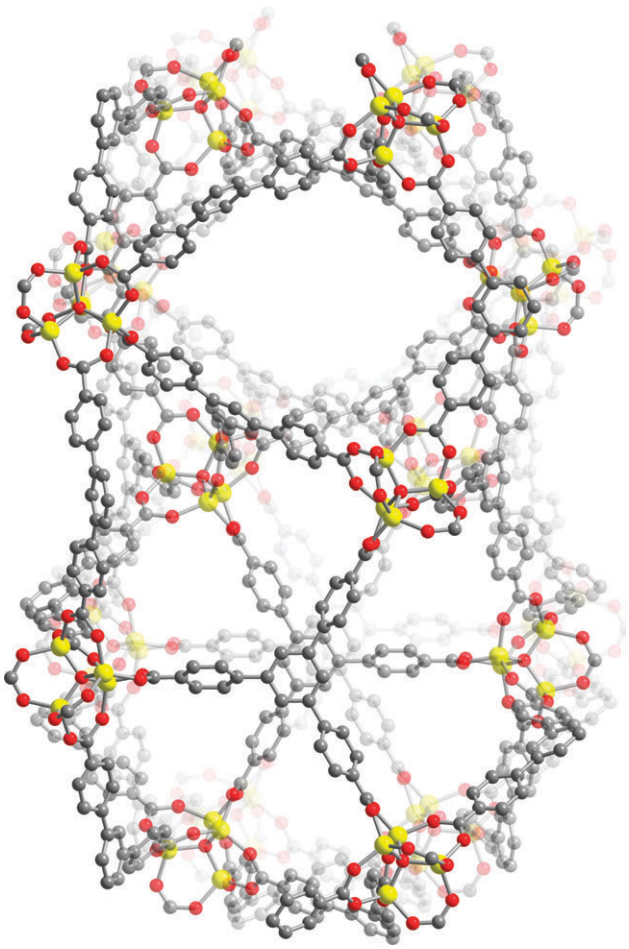

Fig. 3 A portion of the crystal structure of $Zn_4O(BTB)_3$ (MOF-177).[66] Yellow, gray, and red spheres represent Zn, C, and O atoms, respectively; H atoms are omitted for clarity. The structure consists of six diamond-shaped channels (upper), with a diameter of 10.8 Å, surrounding a pore containing eclipsed BTB^{3-} moieties (lower). For the latter, the separation between the central benzene rings of BTB^{3-} can accommodate a sphere with a diameter of 11.8 Å.

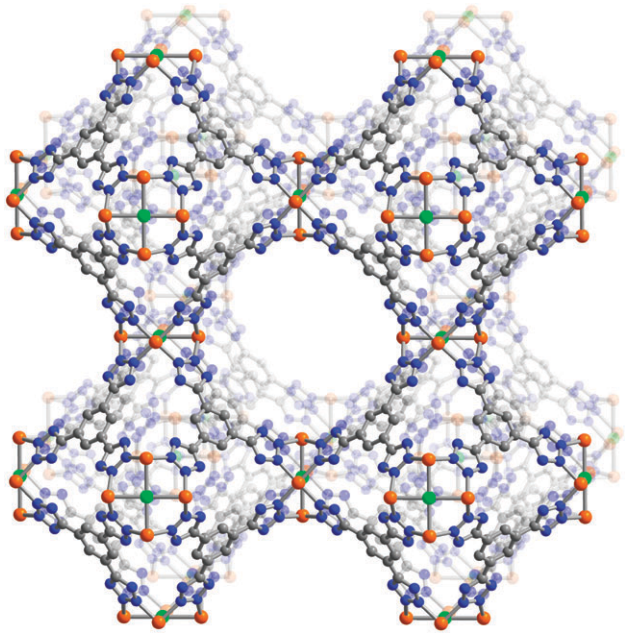

Fig. 4 A portion of the crystal structure of $Mn_3[(Mn_4Cl)_3(BTT)_8]_2$ (Mn–BTT).[21] Orange, bright green, blue, and gray spheres represent Mn, Cl, N, and C atoms, respectively. Charge balancing Mn^{2+} guest cations, H atoms, and solvent molecules attached to the framework Mn^{2+} ions within are omitted for clarity. The structure consists of truncated octahedral cages that share square faces, leading to pores of *ca.* 10 Å diameter.

density of just 49 g L^{-1}. Ultimately, as the volume fraction of space taken up by a framework shrinks toward zero, its total gravimetric uptake will tend toward infinity. This limit of course represents the storage capacity achieved by simply compressing H_2 gas within an empty volume.

While $Zn_4O(BDC)_3$ exhibits excellent hydrogen storage characteristics at 77 K, its performance at 298 K is poor due to the weak interactions between H_2 and the framework. Indeed, its volumetric storage capacity at 100 bar and 298 K is 9.1 g L^{-1},[19] barely greater than the density of pure H_2 gas compressed under these conditions (7.7 g L^{-1}).[79] As discussed above, open metal coordination sites on the framework surface can increase the strength of H_2 adsorption, resulting in an improved performance at 298 K. This was first demonstrated in $Mn_3[(Mn_4Cl)_3(BTT)_8]_2$, which contains open Mn^{2+} coordination sites (see Fig. 4) and exhibits an isosteric heat of H_2 adsorption of 10.1 kJ mol^{-1} at zero coverage.[21] Here, powder neutron diffraction data revealed a strong Mn–D_2 interaction, with a separation between the metal and the center of the D_2 molecule of just 2.27 Å. This is a much shorter distance than the >3 Å normally observed for physisorbed hydrogen,[80] and presumably contributes to a more efficient packing of hydrogen molecules in the pores. As a result, the compound exhibits a volumetric storage capacity of 60 g L^{-1} at 90 bar and 77 K, despite having a BET surface area of just 2100 m^2 g^{-1}. Most notably, however, at 90 bar and 298 K, a capacity of 12.1 g L^{-1} was observed (see Fig. 5). This is 77% greater than the density of compressed H_2 gas under these conditions, and represents the current record for a metal–organic framework.

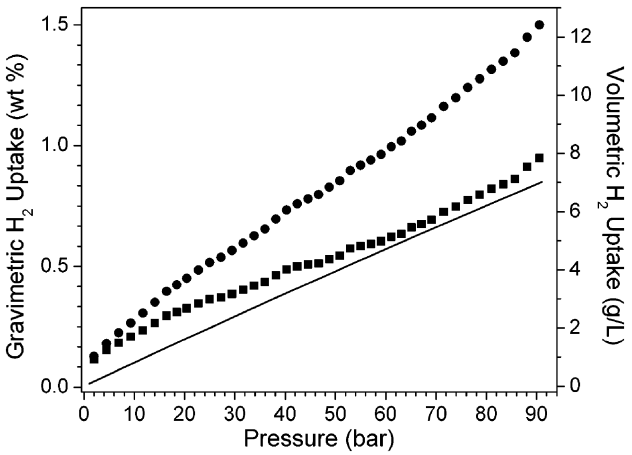

Fig. 5 Excess (squares) and total (circles) hydrogen uptake for $Mn_3[(Mn_4Cl)_3(BTT)_8]_2$ at 298 K.[21] The solid line represents the density of compressed hydrogen over the given pressure range at this temperature.

Significant improvements in room-temperature performance are expected if similar frameworks can be generated with exposed metal centers that have a slightly stronger interaction with H_2 and are present on the surface at a higher concentration. To date, the highest isosteric heat of H_2 adsorption reported for a metal–organic framework is 12.3(5) kJ mol^{-1}, as observed in $Zn_3(BDC)_3[Cu(Pyen)]$ (H_2Pyen = 5-methyl-4-oxo-1,4-dihydro-pyridine-3-carbaldehyde).[81] Although direct evidence of H_2 binding to metal centers is not available for this compound, coordinatively-unsaturated Cu^{2+} sites attached to salen-type ligands are thought to be responsible for the high adsorption enthalpy. The strongest interaction energy yet observed for an individual H_2 binding site is 13.5 kJ mol^{-1} in Ni_2(dhtp) (H_4dhtp = 2,5-dihydroxyterephthalic acid), as observed by variable-temperature infrared spectroscopy (see below for further details).[82]

The foregoing compounds represent the current state-of-the-art for hydrogen storage in metal–organic frameworks. Although none of the materials simultaneously meet all of the targets set by the US Department of Energy, they are within range for a number of key characteristics, suggesting that a logical approach may indeed produce related compounds with exceptional H_2 storage properties.

Structure–performance correlations

Carboxylate-based frameworks

The vast majority of the frameworks listed in Table 1 are constructed from multitopic ligands bearing the carboxylate functionality. Most of these carboxylate-based ligands are either commercially available, such as the ubiquitous 1,4-benzenedicarboxylate (BDC^{2-}) and 1,3,5-benzenetricarboxylate (BTC^{3-}), or easily accessible through well-defined and high-yielding synthetic pathways. Carboxylic acids are also attractive as framework-forming reagents because their high acidity ($pK_a \cong 4$) allows facile *in situ* deprotonation. Relatedly, the metal–carboxylate bond formation is reversible under relatively mild conditions, which presumably facilitates

the formation of well-ordered, crystalline metal–organic frameworks.

While accessibility and favorable thermodynamics make carboxylic acids the most popular ligand choice even today, it was perhaps the extensive literature on molecular metal–carboxylate systems that inspired initial work with these ligands.[83] For instance, Yaghi and coworkers mimicked the structure of basic zinc acetate, $Zn_4O(O_2CCH_3)_6$, to produce $Zn_4O(BDC)_3$ and a plethora of other frameworks bearing the same tetrahedral cluster motif.[65] Interestingly, although structurally analogous $M_4O(O_2CR)_6$ (M = Be, Co) molecules are well-established,[83] metal–organic frameworks containing such units are still unknown. Given the position of $Zn_4O(BDC)_3$ as one of the best performers for hydrogen storage, routes to the analogous $Be_4O(BDC)_3$ and $Co_4O(BDC)_3$ frameworks would be of great interest to the community. Indeed, the beryllium-containing compound would be expected to display a total gravimetric storage capacity *ca.* 4.1 wt% higher than that of $Zn_4O(BDC)_3$ at 100 bar, owing to its lighter-weight framework. Unfortunately, however, concerns over toxicity render beryllium-containing compounds unlikely candidates for a widespread fuel-storage application. Thus, an analogous $Mg_4O(BDC)_3$ framework would perhaps be of greater utility. While Mg^{2+} has essentially the same ionic radius as Zn^{2+}, its solution chemistry is distinctly different, and even tetrahedral $Mg_4O(O_2CR)_6$ molecules have not yet been realized.

Despite the great promise for high gravimetric hydrogen uptake in metal–organic frameworks based on light main group metal ions, such as Be^{2+}, Mg^{2+}, Al^{3+}, and Ca^{2+}, these remain relatively few in number. No porous beryllium-containing frameworks have been reported to date. Of the few known magnesium frameworks, most exhibit a rather low surface area and consequently the highest H_2 uptake yet reported is just 0.78 wt% at 77 K and 1 bar, as observed for $Mg_3(NDC)_3$.[84] The two aluminium frameworks that have been measured perform somewhat better, with Al(OH)(BDC) exhibiting an excess gravimetric uptake of 3.8 wt% and a volumetric capacity of 37 g L^{-1} at 16 bar and 77 K.[85] To our knowledge, no calcium-based metal–organic frameworks have yet been shown to exhibit microporosity.

Transition metal–carboxylate frameworks have received by far the most attention, with the majority of studies focusing on Cu^{2+}- or Zn^{2+}-containing compounds. Of particular interest are compounds exhibiting a high surface area for gas adsorption. We note that these tend to be high-symmetry structures involving rigid bridging ligands and robust metal cluster nodes. A high degree of framework connectivity and strong metal–ligand bonds appear to be necessary for maintaining the framework architecture under the conditions required to evacuate the solvent from the pores. In this regard, the bridging bidentate coordination ability of carboxylate groups looks to be of chief importance. Indeed, the aforementioned tetrahedral $Zn_4O(O_2CR)_6$ units serve as nodes in many of the highest-surface area frameworks. For example, $Zn_4O(BDC)_3$ (see Fig. 1) and $Zn_4O(BTB)_2$ (see Fig. 3) display BET surface areas of 3800 and 4750 m^2 g^{-1}, respectively,[19,66,69,78] which, as discussed above, result in exceptionally high hydrogen storage capacities at 77 K. Other notable materials include $Cr_3OF(BDC)_3$[86] and $Cu_2(qptc)$ ($qptc^{4-}$ = quaterphenyl-3,3′′′,5,5′′′-tetracarboxylate),[87] which feature oxo-centered triangular and paddlewheel-type clusters, respectively. At 77 K, the former compound exhibits a Langmuir surface area of 5500 m^2 g^{-1} and an excess H_2 uptake of 6.1 wt% at 80 bar, while the latter exhibits a BET surface area of 2930 m^2 g^{-1} and an excess H_2 capacity of 6.1 wt% at 20 bar.

While there are numerous examples of carboxylate-bridged frameworks with high H_2 uptake capacities at 77 K, the majority of these display isosteric heats of adsorption below 6–7 kJ mol^{-1}. This is due to the fact that many metal–carboxylate building units, and most notably tetrahedral $Zn_4O(O_2CR)_6$ units, lack coordinatively-unsaturated metal centers. The utility of using exposed metal sites is evident in the large number of carboxylate-based frameworks containing the paddlewheel motif, $Cu_2(O_2CR)_4$. Here, each Cu^{II} center can potentially lose a terminal solvent ligand bound in the axial position, thereby providing an open coordination site for H_2 binding. The prototypical material of this type is $Cu_3(BTC)_2$, which adopts the structure depicted in Fig. 6. Indeed, this metal–organic framework was one of the first shown to bind hydrogen at metal sites at low temperatures, as demonstrated using variable-temperature infrared spectroscopy[82] and powder neutron diffraction data.[88] Among paddlewheel-based frameworks, particularly impressive results were recently reported for $Cu_6(C_s\text{-mdip})_2(C_{2v}\text{-mdip})$, which adsorbs 3.05 excess wt% of H_2 at 1 bar and 77 K.[89] Although definitive proof of metal–H_2 binding and a binding energy profile were not reported for this compound, the authors attribute the unusually high H_2 uptake to overlapping attractive potentials from multiple Cu_2 paddlewheel units.

Numerous different metal cluster structure types could act as building units for carboxylate-based frameworks.[41] There are, however, only a few examples of isomorphous

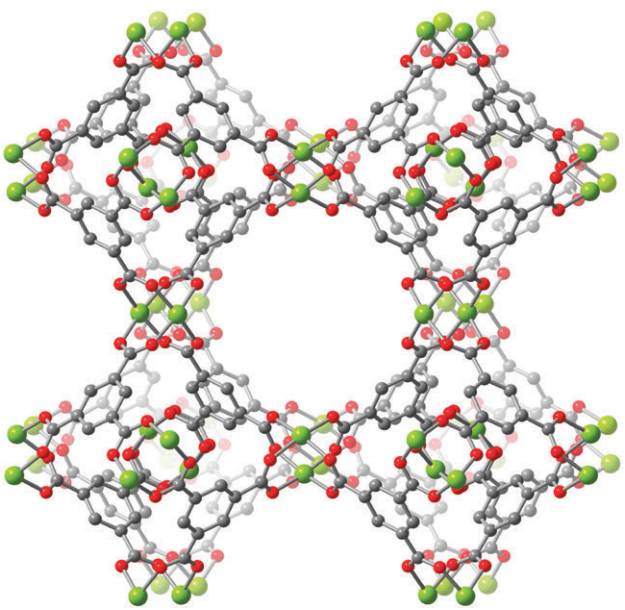

Fig. 6 A portion of the crystal structure of $Cu_3(BTC)_2$ (HKUST-1).[121] Green, gray, and red spheres represent Cu, C, and O atoms, respectively; H atoms are omitted for clarity. Similar to Mn-BTT, the structure consists of octahedral cages that share paddlewheel units to define pores of *ca.* 9.8 Å diameter.

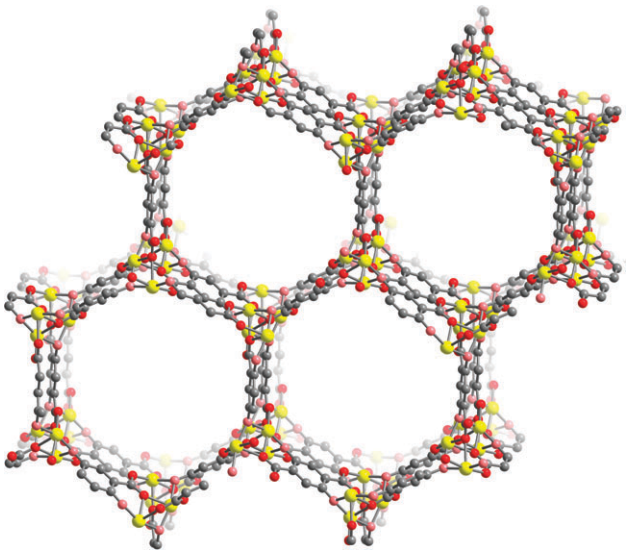

Fig. 7 A portion of the crystal structure of desolvated Zn_2(dhtp).[122] Yellow, gray, red, and pink spheres represent Zn, C, carboxylate O, and alkoxide O atoms, respectively; H atoms are omitted for clarity. The extended solid contains hexaganol channels approximately 9.8 Å wide. Each Zn^{2+} ion is coordinated by two carboxylate and two alkoxide O atoms in the equatorial plane, with the open axial coordination site, previously occupied by solvent, oriented toward the channel interior.

frameworks for which hydrogen storage data exist, and, as such, drawing conclusive structure–property relationships is difficult. Of particular interest here are isomorphous systems supporting open metal coordination sites. Hence, the synthesis of new frameworks based on paddlewheel $M_2(O_2CR)_4$ or triangular $M_3O(O_2CR)_6$ clusters, which are known in molecular chemistry to form for a wide range of metal centers, can be anticipated to provide exciting results. Relatedly, variation of the metal within the M_2(dhtp) structure type shown in Fig. 7 has been demonstrated recently,[90–94] and measurements on these compounds should afford valuable insight into the nature of H_2 binding to metal centers in metal–organic frameworks.

Heterocyclic azolate-based frameworks

A functional analogue of the carboxylate group is tetrazolate, a five-membered heterocyclic ring with four adjacent nitrogen atoms that is easily accessible *via* a [2 + 3] dipolar cycloaddition between organic cyanide, R–C≡N, and the azide anion, N_3^-. Akin to a carboxylic acid moiety, deprotonation of the tetrazole ring occurs at a pH of approximately 4. As such, the monoanionic tetrazolate functionality, $-CN_4^-$, can be synthesized *in situ* under conditions that are very similar to those used with carboxylic acids. The similarity between tetrazolates and carboxylates extends to their coordination chemistry, and there are indeed examples of tetrazolate-based frameworks that emulate the structure of their carboxylate-based analogues. Two such examples are $Zn_3(BDT)_3$ (BDT^{2-} = 1,4-benzeneditetrazolate) and $Cu[(Cu_4Cl)(ttpm)_2]_2$ ($ttpm^{4-}$ = tetrakis(4-tetrazolylphenyl) methane), which are structural analogues of $Zn_3(BDC)_3$ and $Cd_4(TCPM)_2$ ($TCPM^{4-}$ = tetrakis(4-carboxyphenyl)methane),[95] respectively, and which adsorb 1.46 and 2.8 excess wt% of H_2, respectively, at 1 bar and 77 K.[96,41] Unfortunately, H_2 sorption data for the carboxylate-based analogues have not been reported in these cases, and are further absent for other tetrazolate–carboxylate framework analogues.

Despite their similarities in chemical behavior, the two functionalities also differ in several ways. One of these is the ability of tetrazolate ligands to use two, three, or all four nitrogen atoms for metal coordination, in contrast to carboxylates, which are typically bidentate. The varied coordination modes of the tetrazolate group can therefore give rise to structures that are not accessible with carboxylate ligands. In addition, when coordinating through the N3 and N4 atoms, the pinched donor atom geometry of tetrazolate relative to the O atoms of carboxylate can favor the isolation of coordinatively-unsaturated metal centers.[96] This attribute is most prominently displayed in $Mn_3[(Mn_4Cl)_3(BTT)_8]_2$ and its guest cation-exchanged variants, which exhibit initial isosteric heats of H_2 adsorption of up to 10.5 kJ mol^{-1}.[28] Interestingly, the analogous copper(II)-containing framework, $HCu[(Cu_4Cl)_3(BTT)_8]$, displays a significantly reduced initial isosteric heat of adsorption of 9.5 kJ mol^{-1}. The weaker binding of the metal-bound solvent molecules within this framework, however, enables its complete desolvation, such that at higher H_2 loadings the heat of adsorption surpasses that of the Mn-BTT framework. For comparison purposes, it would certainly be of value to generate further analogues of this structure type containing other divalent metal ions.

While both carboxylate- and tetrazolate-based frameworks can exhibit moisture sensitivity, the latter can also suffer from a reduced thermal stability. Thus, most tetrazolate-based frameworks start to collapse above 200 °C, making them more difficult to desolvate without structural deformation. The detrimental effect of increased temperature can to some extent be circumvented by employing milder desolvation techniques. For example, exchange of high-boiling DMF with methanol, followed by desolvation at only 65 °C leads to a total H_2 uptake of 4.5 wt% and 37 g L^{-1} for $Mn_3[(Mn_4Cl)_3(tpt\text{-}3tz)_8(DMF)_{12}]_2$ at 80 bar and 77 K.[50]

Ultimately, the temperature and moisture sensitivity of tetrazolate-based frameworks make these non-ideal candidates for hydrogen storage applications. Stability problems can potentially be addressed, however, by replacing tetrazole with related five-membered azole rings, such as triazole, pyrazole, and imidazole. The higher pK_a values for these heterocycles, 9–10 for triazoles and 14–15 for pyrazole and imidazole,[97] translate into an increased nucleophilicity for their conjugate bases and much-improved strength of the ensuing metal–nitrogen bond. In principle, 1,2,3-triazole and pyrazole could be used to construct geometric analogues of the bridging tetrazolate ligands, enabling synthesis of more stable analogues of the known tetrazolate-based frameworks. In one such example, 1,4-benzenedi(4′-pyrazole) (H_2BDP) was used to synthesize Co(BDP) (see Fig. 8), which is structurally related to Cu(BDT). As opposed to Cu(BDT), which is not thermally stable and does not show significant H_2 uptake upon desolvation,[96] Co(BDP) is stable to 400 °C and can adsorb large amounts of H_2.

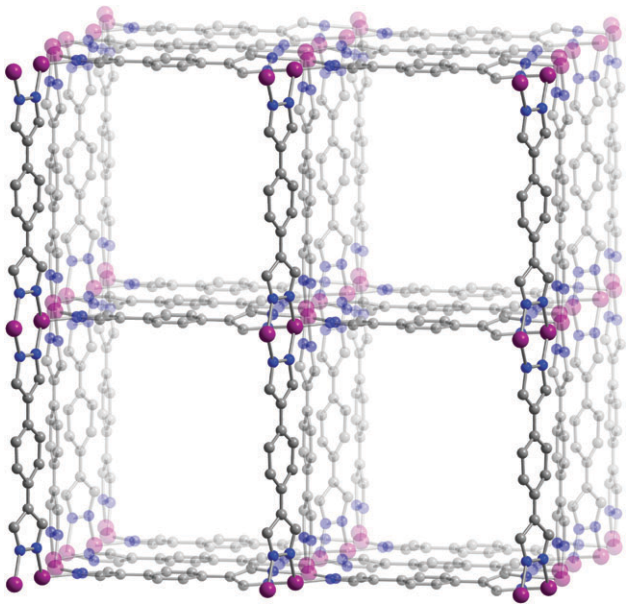

Fig. 8 A portion of the crystal structure of Co(BDP).[37] Purple, gray, and blue spheres represent Co, C, and N atoms, respectively. Upon desolvation, the square channels (*ca.* 12 Å wide) are proposed to collapse in a manner similar to an accordion. Gas adsorption results in a stepwise reopening of the pores.

Unlike the majority of the frameworks discussed here, Co(BDP) is an example of a flexible metal–organic framework. Upon desolvation, its structure changes substantially, but without loss of framework connectivity. At 77 K, it exhibits almost no H_2 uptake up to 20 bar, whereafter a sharp adsorption step occurs, leading to an excess adsorption of 3.1 wt%.[37] Loss of H_2 then occurs only below 15 bar, such that the adsorption and desorption steps define a broad hysteresis loop (see Fig. 9). More subtle versions of this effect have been observed for other flexible frameworks;[35,85,98] however, at 2670 m^2 g^{-1}, Co(BDP) has the largest Langmuir surface area yet reported for such a compound. Importantly, if the effect could be brought into the right range of activation energies, materials of this type could perhaps provide a means of storing H_2 *via* a kinetics-based trapping mechanism. This would be akin to proposed storage schemes involving hydrogen clathrates,[99–101] but with materials that could potentially function at more accessible H_2 loading pressures.

Similar to pyrazole, imidazole can give rise to very robust metal–organic frameworks. Several imidazolate frameworks have been shown to exhibit impressive stability to both chemical agents, such as concentrated basic solutions, and to temperatures in excess of 350 °C.[29] Despite the large number of imidazolate-based frameworks reported thus far, hydrogen storage data exist for only few of them. Among these, the highest capacity measured is 3.3 excess wt% at 30 bar and 77 K for $Zn(MeIM)_2$ (ZIF-8).[31] While more hydrogen storage data on these compounds will surely be forthcoming, it would be of particular interest to devise methods for generating such stable frameworks that also feature open metal coordination sites.

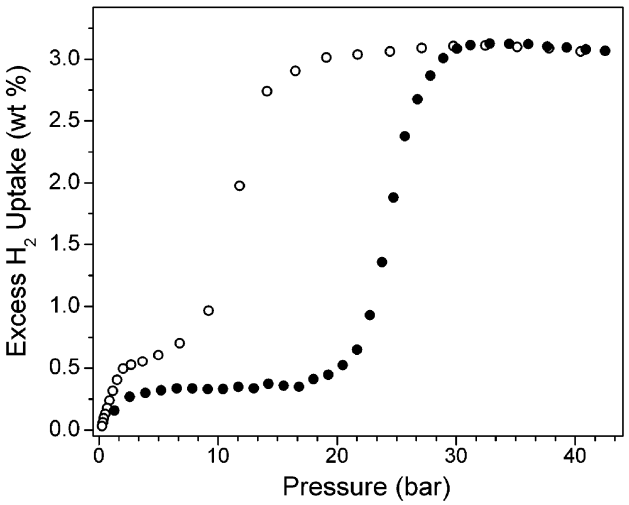

Fig. 9 Hydrogen sorption isotherm for Co(BDP) at 77 K, displaying a broad hysteresis.[37] Adsorption (filled circles) proceeds in a stepwise manner, with the first step reaching a plateau at *ca.* 4 bar and the second at *ca.* 30 bar. Desorption (open circles) occurs at lower pressures, with steps beginning at *ca.* 16 and *ca.* 2 bar.

Mixed-ligand/functionality systems

Another means of addressing the reduced thermal stability of tetrazolate-based frameworks while still taking advantage of the more versatile coordination chemistry of these ligands is to use mixed ligand systems, such as a mixture of carboxylates and tetrazolates. Although it becomes increasingly difficult to design materials that contain two different metal-binding functionalities, frameworks with impressive H_2 storage properties were reported recently using this approach. Most notable among these is $Cu_6O(tzi)_3(NO_3)$ (tzi^- = 5-tetrazolyl-isophthalate), a material constructed from a triangular ligand that possesses two carboxylate groups and a tetrazolate ring.[102] Here, the carboxylate groups serve to construct the well-known paddlewheel $Cu_2(O_2CR)_4$ building unit, while the tetrazolate participates in the formation of a previously unknown metal-building unit, $Cu_3O(N_4CR)_3$. In this triangular cluster, each Cu^{2+} ion exhibits two empty coordination sites, which presumably contribute to a high isosteric heat of adsorption of 9.5 kJ mol^{-1} and an H_2 uptake of 2.4 wt% at 1 bar and 77 K. Similar approaches, where different functionalities target metal-building units of specific geometries, may reduce the serendipity associated with this method, and could potentially lead to particularly complex, but well-engineered and effective H_2 storage materials.

Metal–cyanide frameworks

The H_2 uptake characteristics of metal–cyanide frameworks, perhaps the oldest class of synthetic microporous materials, are of interest owing to the wide range of metal centers that can be exposed on their internal surfaces upon dehydration. The first such compounds studied were the series of Prussian blue analogues of formula $M_3[Co(CN)_6]_2$ (M = Mn, Fe, Co, Ni, Cu, Zn), which contain open M coordination sites as a result of vacancies at the $[Co(CN)_6]^{3-}$ sites within the cubic framework.[44] Amongst these, $Cu_3[Co(CN)_6]_2$ exhibits the

highest H_2 storage capacity, taking up 1.8 excess wt% at 77 K and 1.2 bar. Surprisingly, despite the presence of open metal coordination sites, the highest isosteric heat of adsorption observed for the series was just 7.4 kJ mol^{-1} in $Ni_3[Co(CN)_6]_2$. Thus, it appears that the electronic structure of the N-bound divalent metal ions within these frameworks is not conducive to generating a strong interaction with H_2. It is worth noting, however, that slightly higher H_2 binding energies appear to occur at low loadings within the dehydrated form of Prussian blue itself: $Fe_4[Fe(CN)_6]_3$.[76]

The family of compounds $A_2Zn_3[Fe(CN)_6]_2 \cdot nH_2O$ (A = H, Li, Na, K, Rb, Cs) provided an opportunity for studying the strength of H_2 interactions with alkali metal cations located within the pores of an anionic metal–cyanide framework.[40,103] Upon dehydration, a maximum excess uptake of 1.2 wt% at 77 K and 1.2 bar and a maximum isosteric heat of adsorption of 9.0 kJ mol^{-1} were observed for $K_2Zn_3[Fe(CN)_6]_2$. Most significantly, however, an unexpected trend was observed in the isosteric heats of adsorption, with the values at low coverage decreasing along the sequence $K^+ > (H_3O)^+ > Rb^+ \approx Li(H_2O)^+ > Na^+$. This trend is in distinct contrast to the observations in the gas phase, and suggests that the effective charge of a small guest cation such as Na^+ can be significantly attenuated by it lodging within crevices of a framework surface.

Although the low-pressure H_2 uptake values at 77 K for certain metal–cyanide frameworks are on a par with those of metal–organic frameworks, they are not expected to perform as well at higher pressures. This is because the short cyanide bridge leads to relatively dense framework structures that typically exhibit surface areas below 900 m^2 g^{-1}. In addition, without some means of further increasing their H_2 binding affinity, it is unlikely that they will perform well at 298 K.

Covalent organic frameworks

A recent addition to the family of crystalline microporous materials are the covalent organic frameworks. Unlike metal–organic frameworks, wherein metal ions or clusters make up the nodes of the underlying topological motifs, covalent organic frameworks are by definition devoid of metals and are constructed entirely from strong covalent bonds. Notably, owing to the absence of typically weaker metal–ligand bonds, which render most metal–organic frameworks chemically and thermally unstable, covalent organic frameworks normally exhibit extraordinary thermal and chemical stability, in many ways resembling some high melting-point amorphous polymers. What makes covalent organic frameworks distinct from other organic polymers, however, is that they share many of the same attributes as metal–organic frameworks: they are crystalline and have a well-defined macromolecular structure, they exhibit high porosity, and they have high surface areas. In addition, their crystal structures can be reduced to topologically idealized networks that can potentially be synthesized by design from various combinations of small organic building units.[104]

Given their light weight owing to the absence of heavy metal components, it is not surprising that covalent organic frameworks can adsorb significant amounts of gases, including hydrogen. For instance, at 100 bar and 77 K $C_9H_4BO_2$ (COF-5), a two-dimensional framework obtained by the condensation of 1,4-benzenediboronic acid with hexahydroxytriphenylene, exhibits excess and total H_2 uptake capacities of 3.3 and 5 wt%, respectively.[15] Volumetrically, however, only 33 g L^{-1} of H_2 are stored within COF-5, a rather low value that is associated with the low density of the material. In fact, the extraordinary gravimetric capacities that are predicted for existing frameworks (almost 20 wt% calculated for $(C_{18}H_6O_6)_4(C(C_6H_4B)_4)_3$, COF-108) are offset by volumetric capacities that are not expected to exceed 50 g L^{-1} at 100 bar and 77 K.[12,15] Nevertheless, it is clear that it should be possible to design a covalent organic framework with a volumetric storage density at least matching the 66 g L^{-1} observed for $Zn_4O(BDC)_3$ under these conditions. This would require development of a synthetic route to a framework exhibiting an equivalent, or perhaps even improved, pore dimension profile. As discussed above, the optimal distance between surfaces for high-density hydrogen storage at 77 K is predicted to be 10 Å. Since covalent organic frameworks do not possess strong surface dipoles, doping with metal species would provide the most likely means of generating materials exhibiting good storage characteristics at 298 K.[11,17,105,106]

Characterization of framework–H_2 interactions

Unlike activated carbons and other graphitic structures, metal–organic frameworks exhibit highly heterogeneous van der Waals potentials within their pores. Therefore, H_2 molecules show preference for particular loci, such as open metal sites or metal-building units. At low temperatures, weaker adsorption sites, such as the aromatic rings on organic linkers, become occupied only after these stronger binding sites are saturated. A detailed understanding of the localization of H_2 within metal–organic frameworks is clearly important for developing materials that can function at temperatures closer to room temperature. In particular, neutron diffraction, inelastic neutron scattering, and infrared spectroscopy have been used to explore the site-specific interactions of hydrogen within a framework and the energetics of those binding events.

Neutron diffraction and inelastic neutron scattering

Powder neutron diffraction patterns recorded for desolvated samples of a framework at low temperature under a pressure of D_2 can provide precise spatial resolution of hydrogen binding sites. The preference, and consequently the relative binding energies, of hydrogen for sites within the framework can be determined by monitoring the occupancy of each site as a function of D_2 loading. At high loadings, the overall availability of the site for hydrogen adsorption can also be assessed.

Inelastic neutron scattering (INS) spectroscopy, in which the collision of neutrons with bound hydrogen results in rotational excitation of the H_2 molecule, can give information on the number of individual binding sites as a function of H_2 loading, and in principle can inform on the binding energy of each site. However, an INS absorption band cannot be

unequivocally assigned to a particular location, and peaks with the highest rotational barrier are assigned to H_2 bound at/near metal clusters. Computational methods are often used in conjunction with INS spectra to confirm band assignments and to calculate the adsorption energy and the H_2 orientation at a given site within the solid.

Both of these neutron techniques have been performed on $Zn_4O(BDC)_3$ (see Fig. 1). INS spectra recorded for different temperatures at loadings of less than 8 H_2 per formula unit display two peaks centered at 10.3 and 12.1 meV (a lower value corresponds to a larger rotational barrier).[65] These peaks were assigned to H_2 bound to the Zn_4O cluster unit and the BDC^{2-} linker, respectively. Higher H_2 loadings revealed a splitting of the 12.1 meV absorption band, indicating that multiple binding sites exist for which adsorbed H_2 molecules have similar rotational barriers. The INS data, and subsequent neutron diffraction experiments coupled with a series of computational studies,[107–110] confirmed that the three strongest binding sites are near the Zn_4O cluster (*i.e.*, are near the corners within the cubic framework) and the fourth site is a weaker interaction with the aromatic ring. These data further revealed that at high loadings the H_2 molecules form cages, wherein they are situated less than 3.0 Å from each other. This distance is below the intermolecular $H_2\cdots H_2$ separation observed in solid hydrogen, and supports the better packing efficiency observed within $Zn_4O(BDC)_3$ at high pressures compared to liquid and solid H_2. As expected based on the analogous structural motifs, binding sites that are similar in nature to those observed for $Zn_4O(BDC)_3$ were also determined by neutron techniques for the isoreticular frameworks $Zn_4O(NDC)_3$, $Zn_4O(bpdc)_2$, $Zn_4O(hpdc)_3$, and $Zn_4O(BTB)_2$.[110]

Neutron diffraction experiments have further been employed to demonstrate hydrogen binding to open metal coordination sites. For instance, recent studies performed on Zn_2(dhtp) (see Fig. 7) elucidated three binding sites that are occupied below 30 K.[111] The highest affinity site is located near the Zn^{2+} ion, with a Zn^{2+}–D_2 distance of *ca.* 2.6 Å. Variable-temperature INS experiments gave an estimated binding energy for this site of 8.8 kJ mol^{-1}. Hydrogen molecules were also observed to bind to two additional sites by weaker dispersive forces. For the stronger of these two sites, three of the oxygen atoms coordinated to Zn^{2+} interact with a D_2 molecule at a separation of 3.1 Å, resulting in an estimated adsorption energy of 5 kJ mol^{-1}. At the weaker adsorption site, the distance between the aromatic ring of the dihydroxyterephthalate linker and a D_2 molecule is 3.3 Å, in line with that of a typical van der Waals interaction. Interestingly, the ensemble of adsorbed hydrogen molecules at the three sites gives rise to a "one-dimensional tubular structure" with intermolecular distances comparable to those observed in $Zn_4O(BDC)_3$.

Neutron diffraction and variable-temperature INS experiments carried out on $Cu_3(BTC)_2$ (see Fig. 6) revealed six different hydrogen adsorption sites.[88,112] The vacant axial coordination sites of the Cu^{II} centers bind D_2 at a separation of just 2.39 Å. From INS studies, the hydrogen at this site has a large rotational barrier, consistent with the estimated binding energy of just 6–10 kJ mol^{-1}. Subsequent adsorbate molecules occupy sites within the small cages first and then the large channels, binding to the aromatic linker and the oxygen atoms of the carboxylate groups in both locations. Neutron diffraction experiments performed at high D_2 loadings indicate that the lattice parameters of the framework undergo minor changes, which possibly arise from bending of the BTC^{3-} unit. Similarly, the absorption peak in the INS spectra corresponding to hydrogen bound in the small pocket shifts to higher energy at high loadings, suggesting that hydrogen binding indeed provokes minor changes in the environment of this adsorption site.

Hydrogen was also observed to bind directly to the open metal coordination sites in $Mn_3[(Mn_4Cl)_3(BTT)_8]_2$ (see Fig. 4) and its copper analogue, $HCu[(Cu_4Cl)_3(BTT)_8]$, at low temperature. Here, D_2 interacts with the metal ions at distances of 2.27 Å (Mn^{2+})[21] and 2.47 Å (Cu^{2+}).[27] The short Mn–D_2 separation represents the closest contact yet observed for hydrogen with the surface of a metal–organic framework. A second strong adsorption site occurs in these structures, at which D_2 resides within a pocket created by a Cl^- anion and four tetrazolate rings. Two additional weaker adsorption sites associated with the bridging ligands were also observed in each case. At the highest D_2 loadings measured, almost complete saturation was observed for the site adjacent to the Cu^{2+} ions, indicating that these sites are indeed all open and available for binding hydrogen.

A low-temperature neutron diffraction study of Y(BTC) shows that open metal coordination sites within a metal–organic framework are not always the strongest adsorption sites for hydrogen.[113] A similar result was obtained for $Cu_3[Co(CN)_6]_2$, wherein neutron diffraction showed that the Cu^{2+} ions provided only the second strongest adsorption site.[114] The measurements performed on Y(BTC) indicate that at low D_2 loadings the adsorbate binds first to the aromatic ring of the BTC^{3-} linker, with a separation of 3.7 Å. At higher loadings, a D_2 adsorption site located 4.27 Å from the Y^{3+} ion was observed. It was proposed that the small pore size of only 5.8 Å in this material gives rise to dispersive interactions that are stronger than the interaction with the metal ion, accounting for the weaker preference for the open metal coordination site in this material. Two other low affinity sites are observed at higher H_2 loadings, but the adsorption enthalpy of these sites are significantly weaker (<4 kJ mol^{-1}). As observed in other frameworks, the intermolecular distance between adsorbed hydrogen molecules is shorter (2.86 Å) than the distance in solid D_2.

Other frameworks have also been analyzed using these neutron methods, including $NaNi_3(OH)(sip)_2$ and the Prussian blue analogues $M_3[Co(CN)_6]_2$, (M = Mn, Fe, Co, Ni, Cu, Zn).[114–116] In the metal–cyanide frameworks, it has been proposed that the adsorption enthalpy is dependent on the pore size in relation to the kinetic diameter of the hydrogen molecule, and is not governed solely by the nature of the M^{2+} ion.[115]

Variable-temperature infrared spectroscopy

Unperturbed H_2 is infrared inactive, but shows Raman bands at ν_{H-H} = 4161 and 4155 cm^{-1} for para- and ortho-hydrogen,

respectively.[117] Association of H_2 molecules with the surface of a framework, however, polarizes the H–H bond, causing the vibrational transition to become infrared active. The strength of the interaction between H_2 and a binding site, such as a metal ion or an aromatic ring, determines the bathochromic shift of this transition, with stronger binding interactions resulting in a greater shift from the unperturbed system. Hydrogen bound at any available site within a given framework can therefore be observed by infrared spectroscopy. Furthermore, the binding energy for a specific site can be accurately measured from the isobaric temperature dependence of the intensity of the respective absorption band.[117,118] It must be emphasized that this technique probes the interaction of H_2 with the framework in a site-specific manner, which contrasts the isosteric heat of adsorption determined at low H_2 coverage. The latter is an average measure of all sites occupied at that temperature and pressure, and is unable to differentiate between any of these sites.

Hydrogen uptake in $Zn_4O(BDC)_3$ has been investigated using infrared spectroscopy, resulting in the observation of two transitions at 4112 and 4121 cm^{-1} at low pressures.[119] These transitions were assigned to para- and ortho-hydrogen coordinated at the same type of site within the framework. As the H_2 pressure was increased, the two transitions became obscured by a broad absorption band centered at 4130 cm^{-1}. Note that the observed peaks are weakly red-shifted from the unperturbed transitions, indicating that hydrogen does not undergo dissociative adsorption. Moreover, a specific site with a strong binding energy, such as might be expected for H_2 binding directly to a Zn^{2+} ion, was not observed. Indeed, the binding energies determined for the low- and high-pressure sites were 7.4 and 3.5 kJ mol^{-1}, respectively.

Infrared spectroscopy also provided the first strong evidence for H_2 binding to a metal site within a metal–organic framework. Thus, at a low H_2 loading, two transitions at 4097 and 4090 cm^{-1}, which arise from para- and ortho-H_2 binding at one type of site, were observed on $Cu_3(BTC)_2$.[82] The binding energy calculated from variable-temperature measurements for this site is 10 kJ mol^{-1}. This strong adsorption site was assigned to H_2 interacting with the exposed Cu^{2+} ions of the framework based on the frequency of this transition and the magnitude of the binding energy.

Recently, infrared studies were carried out on Ni_2(dhtp), the Ni^{2+} analogue of MOF-74 (see Fig. 7).[120] In this compound, H_2 was observed to adsorb at the coordinatively-unsaturated nickel(II) sites at a relatively high temperature of 180 K with a strong adsorption enthalpy of 13.5 kJ mol^{-1}. Two vibrational frequencies were observed at 4035 and 4028 cm^{-1}, relatively low values demonstrative of the strong interaction between H_2 and the framework. These absorptions correspond to two distinct binding sites and *not* bound ortho/para-hydrogen as observed in Cu_3BTC_2. For the two sites, the hydrogen molecule eclipses an Ni–O bond, where the oxygen atom arises either from the carboxylate or alkoxide group. As the loading of H_2 is increased, two new bands at ν_{H-H} = 4132 and 4120 cm^{-1} are observed, which arise from hydrogen bound to the aromatic linkers.

Conclusions

Since hydrogen storage was first reported in a metal–organic framework, significant and continual progress has been made. In the last few years, marked increases in both the binding energy and the storage capacity have been reported. Specific chemical features, such as high surface areas, vacant coordination sites on metal ions, and strong surface dipole moments, have been demonstrated to enhance hydrogen uptake. Still, significant further advances will be required in order to meet the US DoE targets for an on-board hydrogen storage system.

Metal–organic frameworks can display outstanding performance characteristics for cryogenic hydrogen storage at 77 K and pressures up to 100 bar. In particular, a rapid and fully-reversible H_2 uptake of 10.0 total wt% and 66 g L^{-1} has been observed for $Zn_4O(BDC)_3$.[19] Improvements in gravimetric capacity without loss of storage density can be expected if analogous structures can be constructed from lighter-weight components, as perhaps achievable in $Mg_4O(BDC)_3$ or a covalent organic framework with similar pore dimensions. Improvements in volumetric storage density might also be possible for framework structures exhibiting a consistent 10 Å separation between opposing pore walls. Unfortunately, without strong surface dipoles, it is unlikely that these materials would also function well for hydrogen storage at 298 K.

By generating frameworks bearing open metal coordination sites, it is possible to increase the affinity of the surface for H_2, giving rise to a higher storage capacity at 298 K. For example, exposed Mn^{2+} coordination sites within $Mn_3[(Mn_4Cl)_3(BTT)_8]_2$ contribute to its record uptake of 1.49 total wt% and 12.1 g L^{-1} at 298 K and 90 bar.[21] Here, serious advances in synthetic chemistry are needed to improve performance. The challenge is to design bridging ligands or surface functionalization chemistry that will lead to frameworks with a high concentration of open metal sites, ideally with each metal capable of binding more than one H_2 molecule. The charge density on the metal ions should be sufficient to result in an H_2 binding enthalpy of *ca.* 20 kJ mol^{-1}. Furthermore, to attain gravimetric capacities approaching the DoE targets, it may be necessary to utilize light main group metal ions, such as Li^+, Mg^{2+}, or Al^{3+}.

Some additional factors should be kept in mind when attempting to generate frameworks with improved hydrogen storage properties. Strong metal–ligand bonds within the framework can be critical for ensuring that the material can be fully desolvated without collapsing and is stable to adventitious moisture. Ultimately, a storage material should be cheap to produce and activate on a large scale, and its components should be widely-abundant and should not present an environmental issue upon disposal. Thus, the creation of metal–organic frameworks of true utility for hydrogen storage applications presents a formidable yet exceedingly complex and engaging challenge.

Acknowledgements

This work was supported by the US Department of Energy, the US Defense Logistics Agency, and the General Motors Corporation.

Table 1 Surface area, pore volume, hydrogen storage properties under specific conditions for metal–organic and metal–cyanide frameworks

Compound[a]		Surface area/m^2 g^{-1}		Pore vol./cm^3	Conditions		Hydrogen storage[b]		Q_{st}/kJ mol^{-1}	Ref.
		BET	Langmuir		P/bar	T/K	Excess/wt%	Vol./g L^{-1}		
$Li_{3.2}Mn_{1.4}[(Mn_4Cl)_3(BTT)_8]_2{\cdot}0.4LiCl$		1904	2057		1.2	77	2.06		8.9	28
α-$Mg_3(HCO_2)_6$		150		0.043	1	77	0.6			123
$Mg_3(NDC)_3$	TUDMOF-2		520		1	77	0.78			84
		190			1.12	77	0.46		9.5	124
Al(OH)(BDC)	MIL-53(Al)	1100	1590	0.59	16	77	3.8	37		85
$Al_{12}O(OH)_{18}(H_2O)_3(Al_2(OH)_4)(BTC)_6$	MIL-96				3	77	1.91[c]			125
$Sc(BDC)_3$		721		0.332	1	77	1.5			126
Cr(OH)(BDC)	MIL-53(Cr)	1100	1500	0.56	16	77	3.1			85
$Cr_3OF(BTC)_2$	MIL-100		2700	1	73.3	298	0.15	1.04	6.3	86
					90	77	3.28	23.0		86
$Cr_3OF(ntc)_{1.5}$	MIL-102		42	0.12	35	77	1		6	127
$Cr_3OF(BDC)_3$	MIL-101		5500	1.9	80	298	0.43	1.84	10	86
					80	77	6.1	26.1		86
$Mn(HCO_2)_2$		297[d]			1	77	0.9			128
Mn(NDC)		191		0.068	1	77	0.57			129
$Mn_3[(Mn_4Cl)_3(tpt\text{-}3tz)_8]_2$		1580	1700		25 (80)	77	3.7 (4.5)			50
$Mn_3[(Mn_4Cl)_3(BTT)_8]_2$	Mn-BTT	2100			1.2	77	2.2	43	10.1	21
					90	77	5.1 (6.9)	(60)		21
					90	298	0.94	7.9		
$Mn_3[(Mn_4Cl)_3(BTT)_8]_2{\cdot}0.75CuPF_6$		1911	2072		1.2	77	2.00		9.9	28
$Fe_3(OH)(pbpc)_3$		1200			1	77	1.6			130
					20	77	3.05	33.1		130
$Fe_3O(tfbdc)_3$			635		1	77	0.9			131
$Fe_3[(Mn_4Cl)_3(BTT)_8]_2{\cdot}FeCl_2$		2033	2201		1.2	77	2.21		10.2	28
$Fe_4O_2(BTB)_{8/3}$		1121	1835	0.69	1	77	2.1			132
Co(BDP)			2670	0.93	30	77	3.1			37
Co(HBTC)(4,4′-bipy)		887			1	77	2.05			133
					1	298	0.96			133
Co(NDC)(bpy)			115	0.10	1	77	0.72			134
Co(ox)(bpy)					1	77	0.10			121
$Co_2(6\text{-}mna)_2$	CUK-2	420		0.17	1	77	0.66			135
$Co_2(BDC)_2(dabco)$		1595	2120	0.77	10	298	0.03			136
					44.2	77	4.11			137
					100	293	0.32			137
$Co_3(2,4\text{-}pdc)_2(OH)_2$	CUK-1	630		0.26	1	77	1.60			135
$Co_3(BDC)_3(dabco)$		360	538	0.2	0.93	77	1	51.2		138
$Co_3(bpdc)_3(bpy)$		922		0.38	1	77	1.94		6.9	139
$Co_3[(Mn_4Cl)_3(BTT)_8]_2{\cdot}1.7CoCl_2$		2096	2268		1.2	77	2.12		10.5	28
$Co_3(NDC)_3(dabco)$		1502	2293	0.82	1	77	2.45	29.8		138
					17.2	298	0.89	10.8		138
$H_2[Co_4O(tatb)_{8/3}]$	PCN-9		1355	0.51	1	77	1.53		10.1	140
$NaNi_3(OH)(sip)_2$		743			1	77	0.94		10.4	116
Ni(cyclam)(bpydc)			817	0.37[e]	1	77	1.1			141
$Ni(dhtp)_2$			1083	0.41	70	77	1.8			142
					70	298	0.3			142
Ni(HBTC)(4,4′-bipy)		1590			1	77	3.42			133
					1	298	1.20			133
Ni(ox)(bpy)					1	77	0.16			121
$Ni_2(atc)$					1	77	0.6			143

Table 1 (*continued*)

Compound[a]		Surface area/m^2 g^{-1}		Pore vol./cm^3	Conditions		Hydrogen storage[b]		Q_{st}/kJ mol^{-1}	Ref.
		BET	Langmuir		P/bar	T/K	Excess/wt%	Vol./g L^{-1}		
$Ni_2(bpy)_3(NO_3)_4$				0.181	1	77	0.987			98
$Ni_2(bpy)_3(NO_3)_4$				0.149	1	77	0.653			98
$Ni_{2.75}Mn_{0.25}[(Mn_4Cl)_3(BTT)_8]_2$		2110	2282		1.2	77	2.29		9.1	28
$Ni_3(OH)(pbpc)_3$		1553			1	77	1.99			130
					20	77	4.15	43.9		130
$Ni_3O(tatb)_2$	PCN-5		225		1	77	0.63			144
Cu(BDT)		200			1	77	0.66			96
$Cu(bpy)(CF_3SO_3)_2$					1	40	1.4			145
$HCu[(Cu_4Cl)_3(BTT)_8]\cdot 3.5HCl$	Cu-BTT	1710	1770		1.2	77	2.42		10	27
					90	77	3.7	53.8		27
					80	298	0.46			
Cu(dccptp)(NO_3)		268		0.113	1	77	1.34		6.1	146
					20	77	1.91	23.9		146
$Cu(fum)(bpe)_{0.5}$					1	77	0.8			147
$Cu(2\text{-pymo})_2$		350			1.2	77	0.86	13		148
$Cu(F\text{-pymo})_2$					1.2	77	0.56	10		149
$Cu(hfipbb)(h_2hfipbb)_{0.5}$					48	298	1	14.7		68
					1	77	0.23			121
$Cu_2(C_{2v}\text{-mdip})$	PCN12′	1577	1962	0.73	1	77	2.4	20.4		89
$Cu(C_{2h}\text{-tcppda})$			504		1	77	1.2			150
$Cu(D_{2h}\text{-tcppda})$			626		1	77	1.4			150
$Cu_2(tcpdep)$			733		1	77	0.8			151
$Cu_2(abtc)$	SNU-5			0.89	40–110	77	4.71	53		152
			2850	1	1	77	2.84			153
					50	77	5.22			153
$Cu_2(abtc)(DMF)_2$	SNU-5′		1260	0.48	1	77	1.83			153
$Cu_2(aobtc)$	PCN-10	1407	1779	0.67	1	77	2.34	18	6.8	154
					3.5	30	6.84	52.5		154
					45	300	0.25			154
$Cu_2(BDC)_2(dabco)$		1461			1	77	1.8			73
		1300	1703	0.63	33.7	77	2.7			137
					100	293	0.42			137
$Cu_2(bpndc)_2(bpy)$	SNU-6		2910	1.05	0.92	77	1.68	5.31		155
					70	77	4.87	15.4		155
$Cu_2(bptc)$	MOF-505		1830	0.63	1	77	2.47			156
		1670		0.68	1	77	2.59	38.9		87
					20	77	4.02	37.3		87
$Cu_2(qptc)$		2932		1.14	1	77	2.24	41.1		87
					20	77	6.07			87
$Cu_2(sbtc)$	PCN-11	1931	2442	0.91	1	77	2.55	19.1	7	154
					3.5	30	7.89	59.1		154
					45	77	5.23	39.2		154
$Cu_2(tptc)$		2247		0.89	1	77	2.52	43.6		87
					20	77	6.06			87
$Cu_3(bhtc)_2$	UMCM-150	2300	3100	1	1	77	2.1		7.3	157
					45	77	5.7	36		157

Table 1 (*continued*)

Compound[a]		Surface area/m^2 g^{-1} BET	Surface area/m^2 g^{-1} Langmuir	Pore vol./cm^3	Conditions P/bar	Conditions T/K	Hydrogen storage[b] Excess/wt%	Hydrogen storage[b] Vol./g L^{-1}	Q_{st}/kJ mol^{-1}	Ref.
$Cu_3(BTC)_2$	HKUST-1	1239		0.62	1	77	2.18	213[e]	6.1	158
		1154	1958		50	77	3.6		4.5	67
					65	298	0.35			67
					60	200	1			67
		1507	2175	0.75	1	77	2.48		6.8	122
				0.4	1	77	1.44		6–7	121
					1	77	2.27			159
					10	77	3.6	31.6		159
		1944	2260		77	77	3.3	29		69
$Cu_3[(Cu_{2.9}Mn_{1.1}Cl)_3(BTT)_8]_2{\cdot}2CuCl_2$		1695	1778		1.2	77	2.02		8.5	28
$Cu_3(tatb)_2$ (catenated)	PCN-6		3800		1	77	1.9			48
$Cu_3(tatb)_2$ (non-catenated)	PCN-6′		2700	1.045	1	77	1.35			49
$Cu_3[(Cu_4Cl)_3(tpb\text{-}3tz)_8]_2{\cdot}11CuCl_2$		1120	1200		30	77	2.8			50
$Cu_4(TTPM)_2{\cdot}0.7CuCl_2$		2506	2745		1	77	2.8		8.4	41
					20 (70)	77	4.1 (5.6)	(41)		41
$Cu_6(C_s\text{-}mdip)_2(C_{2v}\text{-}mdip)$	PCN12	1943	2425	0.94	1	77	3.05	23.2		89
$Cu_6O(tzi)_3(NO_3)$			3223		1	77	2.4		9.5	102
$Zn(abdc)(bpe)_{0.5}$			100[d]		1	77	0.62			160
$Zn(BDC)(bpy)_{0.5}$	MOF-508		946		1	77	0.8			161
$Zn(MeIM)_2$	ZIF-8	1630	1810	0.64	1	77	1.27			29
					55	77	3.01			29
					1	77	1.3		4.5	31
					30	77	3.3			31
					60	298	0.13			31
$Zn(NDC)(bpe)_{0.5}$			303	0.2	40	77	2	18		162
					65	298	0.3			162
$Zn(PhIM)_2$	ZIF-11		1676	0.58	1	77	1.35			29
Zn(tbip)		256			1	77	0.75	54	6.7	163
$Zn_2(abtc)(DMF)_2$	SNU-4		1460	0.53	1	77	2.07			153
					50	77	3.70			153
$Zn_2(BDC)(tmbdc)(dabco)$		1100	1670	0.59	1	77	2.08			164
$Zn_2(BDC)_2(dabco)$		1264			1	77	1.92			158
		1165	1488		83.2	77	3.17			137
$Zn_2(bpytc)$		313	424	0.15	4	77	1.1			165
$Zn_2(btatb)$		1370[d]			1	77	2.2		8.1	166
$Zn_2(btatb)(DMF)_2$		796[d]			1	77	1.2		7.4	166
$Zn_2(btatb)(Py)$		709[d]			1	77	1.24			166
$Zn_2(btatb)(MePy)$		370[d]			1	77	0.59			166
$Zn_2(btatb)(EtPy)$		309[d]			1	77	0.57			166
$Zn_2(btatb)(ViPy)$		473[d]			1	77	1.04			166
$Zn_2(btatb)(CF_3Py)$		388[d]			1	77	0.57			166
$Zn_2(cnc)_2(dpt)$			342	0.19	1	77	1.28		7.85	167
$Zn_2(dhtp)$	MOF-74, CPO-27-Zn	783	1132	0.39	1	77	1.75		8.3	122
		950	1072		26.1	77	2.21	27.6		69
		870			30	77	2.8		8.8	111
$Zn_2(NDC)_2(dabco)$		1000	1450	0.52	1	77	1.7			164
$Zn_2(NDC)_2(diPyNI)$			252[d]		1	77	0.2			45
$Zn_2(tcpcdp)$			252[d]		1	77	0.2			151
$Zn_2(tfbdc)_2(dabco)$		1070	1610	0.57	1	77	1.78			164

Table 1 (*continued*)

Compound[a]		Surface area/$m^2\ g^{-1}$		Pore vol./cm^3	Conditions		Hydrogen storage[b]		Q_{st}/kJ mol^{-1}	Ref.
		BET	Langmuir		*P*/bar	*T*/K	Excess/wt%	Vol./g L^{-1}		
$Zn_2(tmbdc)_2(bpy)$		1120	1740	0.62	1	77	1.68			164
$Zn_2(tmbdc)_2(dabco)$		920	1400	0.5	1	77	1.85			164
$Zn_3(BDC)_3(Cu(pyen))$				0.26[e]	1	77	0.66		12.3	81
$Zn_3(BDT)_3$		640			1.17	77	1.46		8.7	96
$Zn_3(bpdc)_3(bpy)$		792		0.33	1	77	1.74		7.1	139
$Zn_3(OH)(cdc)_{2.5}$		152			1	77	2.1		7	168
$Zn_3(tatb)_2(HCO_2)$			1100		1	77	1.3			169
$Zn_3[(Zn_{0.7}Mn_{3.3}Cl)_3(BTT)_8]_2{\cdot}2ZnCl_2$		1927	2079		1.2	77	2.10		9.6	28
$Zn_4(trz)_4(1,4\text{-}ndc)_2$		362			1	77	0.84			32
$Zn_4(trz)_4(NDC)_2$		584			1	77	1.11			32
$Zn_4O(adc)_3$	PCN-13		150	0.1	1	77	0.41			170
$Zn_4O(BDC)_3$	MOF-5, IRMOF-1	2296	3840		50	77	4.7		3.8	67
					65	298	0.28			67
					60	200	0.9			67
					48	298	1.65	9.9		68
		3362			1	77	1.32			66
		3534	4171		45.4	77	4.95	30.8		69
			3080		30	77	4.3		4.1	169
					60	298	0.45			169
		572	1014		67	298	0.2	1.19		70
					10	77	1.6	9.49		70
		2885		1.18	1	77	1.15			71
		3800	4400		40	77	7.1	42.1		19
					100	77	10.0	66		19
					100	298	0.57			19
					1	77	1.32		4.8	31
					30	77	4.3	25.5		31
		1450			1	77	4.5			65
		1794			1	77	2.0			72
					1	77	2.1		5.3	73
$Zn_4O(bpdc)_2$	IRMOF-9	1904	2613	0.9	1	77	1.15			122
$Zn_4O(Brbdc)_2$	IRMOF-2	1722	2544	0.88	1	77	1.5			122
$Zn_4O(BTB)_2$	MOF-177	4526			1	77	1.23	32.1		66
		4746	5640		68.5	77	7.0	32		69
		4750	5640	1.69	66	77	7.1	49		78
$Zn_4O(D_2\text{-tcppda})_{1.5}$			2095		1	77	0.8			172
$Zn_4O(dbdc)_2$	IRMOF-6	2476	3263	1.14	1	77	1.46			122
		2804	3305		45	77	4.63	31.7		69
$Zn_4O(dcbBn)_3$		396		0.13	48	298	0.98			173
$Zn_4O(dcdEt)_3$		502		0.2	48	298	1.12			173
$Zn_4O(H_2Nbdc)_2$	IRMOF-3	2446	3062	1.07	1	77	1.42			122
$Zn_4O(hpdc)_3$	IRMOF-11		1911		1	77	1.59			66
		1984	2337		33.7	77	3.4	26.7	9.1	69
$Zn_4O(NDC)_3$	IRMOF-8	890		0.45	1	77	1.45			158
		1466			1	77	1.48			66
			1818		15	77	3.6	20.9	6.1	171
					30	298	0.4	2.32		171
$Zn_4O(ntb)_2$			1121	0.51	1	77	1.9			174
$Zn_4O(pyrdc)_2$	IRMOF-13	1551	2100	0.73	1	77	1.73			122

Table 1 (*continued*)

Compound[a]		Surface area/m^2 g^{-1} BET	Surface area/m^2 g^{-1} Langmuir	Pore vol./cm^3	Conditions P/bar	Conditions T/K	Hydrogen storage[b] Excess/wt%	Hydrogen storage[b] Vol./g L^{-1}	Q_{st}/kJ mol^{-1}	Ref.
$Zn_4O(tmbdc)_3$	IRMOF-18	1501			1	77	0.88			66
$Zn_4O(ttdc)_2$	IRMOF-20	3409	4346	1.53	1	77	1.32			122
		4024	4593		77.6	77	6.25	34.1		69
$Zn_7O_2(pda)_5(H_2O)_2$				0.17	71.43	298	1.01			175
Y(BTC)					1	77	1.57		7.3	113
$Y_2(pdc)_3$		655			1	77	1.32			176
$Mo_3(BTC)_2$	TUDMOF-1	1280	2010	0.67	1	77	1.75			177
$Pd(2\text{-}pymo)_2$		600			1.2	77	1.3	18	8–9	148
										178
$Pd(F\text{-}pymo)_2$		600			1.2	77	1.15	18		178
$Ag_2[Ag_4(trz)_6]$	FMOF-1	810		0.324	64	77	2.33	41		35
$Cd(pymc)_2$	*rho*-ZMOF		1168	0.47	1	77	1.16		8.7	179
					10	77	2.1	28.8		113
$Cd_3(bpdc)_3$	JUC-48		880	0.19	40	77	2.8	20.0		180
$In_3O(abtc)_{1.5}(NO_3)$	*soc*-MOF		1417	0.5	1.2	77	2.61			181
					1.2	77		50		46
$[In(pmdc)_2Na_{0.36}K_{1.28}](NO_3)_{0.64}$	*sod*-ZMOF		616	0.25	1	77	0.9		8.4	179
$Sm_2Zn_3(oxdc)_6$		719		0.31	34	77	1.19	18.6		182
					35	298	0.54	8.4		182
Dy(BTC)		655			1	77	1.32			183
$Er_2(3,5\text{-}pdc)_3$		427			1	77	0.68			176
$Yb_4(tatb)_{8/3}(SO_4)_2$	PCN-17	820[d]		0.34	1	77	0.94			184
Metal–cyanide frameworks										
$Mn_2[Fe(CN)_6]$					1	77	0.0			76
$Mn_3[Co(CN)_6]_2$		870			1.19	77	1.6	19		44
$Mn_3[Co(CN)_6]_2$					1	77	1.71			185
$Fe_3[Co(CN)_6]_2$		770			1.19	77	1.4	17		44
$Fe_4[Fe(CN)_6]_3$		550			1	77	1.2		6.3–7.6	76
$Co(pyz)[Ni(CN)_4]$					1	77			7.2	186
$Co(pyz)[Pd(CN)_4]$					1	77			7.8	186
$Co(pyz)[Pt(CN)_4]$					1	77			7.6	186
$Co[Fe(CN)_5(NO)]$		523			1	77	1.61		7.5	187
$Co_2[Fe(CN)_6]$		370			1	77	0.7			76
$Co_3[Co(CN)_5]_2$		730			1	77	1.4		5.7–7.0	76
$Co_3[Co(CN)_6]_2$		800			1.19	77	1.5	19		44
$Ni(bpy)[Ni(CN)_4]$		234			1	77	1.84		7.5	186
$Ni(bpy)[Pd(CN)_4]$		220			1	77			7	186
$Ni(dpac)[Ni(CN)_4]$		398			1	77	2.24		6	186
$Ni(pyz)[Ni(CN)_4]$		124			1	77	1.76		7.2	186
$Ni[Fe(CN)_5(NO)]$		634			1	77	1.68		6.5	187
$Ni_2[Fe(CN)_6]$		460			1	77	0.9			76
$Ni_3[Co(CN)_6]_2$		560					1.4	18		44
$Cu_2[Fe(CN)_6]$		730			1	77	1.6		6.0–6.6	76
					1	75	2.22		5.6	185
$Cu_{1.6}Mn_{1.4}[Co(CN)_6]_2$					1	75	2.33		6.3	185
$Cu_{2.3}Mn_{0.7}[Co(CN)_6]_2$					1	75	2.6		6.5	185
$Cu_3[Co(CN)_6]_2$		730			1.19	77	1.8	25		44

Table 1 (*continued*)

Compound[a]	Surface area/$m^2\ g^{-1}$ BET	Surface area/$m^2\ g^{-1}$ Langmuir	Pore vol./cm^3	Conditions P/bar	Conditions T/K	Hydrogen storage[b] Excess/wt%	Hydrogen storage[b] Vol./g L^{-1}	Q_{st}/kJ mol^{-1}	Ref.
$Cu_3[Co(CN)_6]_2$	750			1	77	1.8		6.6–6.8	76
				1	75	2.61		6.9	185
$Cu_3[Fe(CN)_6]_2$				1	75	1.79		7.0	185
$Cu_3[Ir(CN)_6]_2$				1	75	2.39		7.15	185
$Zn_3[Co(CN)_6]_2$	720			1.19	77	1.4	18		44
$H_2Zn_3[Fe(CN)_6]_2{\cdot}2H_2O$				1.19	77	1.1	16	7.8–8.2	40
$Li_2Zn_3[Fe(CN)_6]_2{\cdot}2H_2O$	250			1.19	77	1.1	16	6.1–7.9	40
$Na_2Zn_3[Fe(CN)_6]_2$	570			1.19	77	1.2	18	7.7	40
$Rb_2Zn_3[Fe(CN)_6]_2$	430			1.19	77	1.1	19	7.3–7.9	40
$K_2Zn_3[Fe(CN)_6]_2$	470			1.19	77	1.2	19	7.9–9.0	40
$K_2Zn_3[Fe(CN)_6]_2$				1	75	1.66		8.3	188
$K_2Zn_3[Ru(CN)_6]_2$				1	75	1.5		8.4	188
$K_2Zn_3[Os(CN)_6]_2$				1	75	1.7		8.6	188
$Rb_2Zn_3[Fe(CN)_6]_2$				1	75	1.19		6.8	188
$Rb_2Zn_3[Ru(CN)_6]_2$				1	75	1.3		7.2	188
$Rb_2Zn_3[Os(CN)_6]_2$				1	75	1.4		7.4	188
$Cs_2Zn_3[Fe(CN)_6]_2$				1	75	0.95		6.2	188
$Cs_2Zn_3[Ru(CN)_6]_2$				1	75	1.11		6.9	188
$Cs_2Zn_3[Os(CN)_6]_2$				1	75	1.1		7.1	188
$Ga[Co(CN)_6]$	570			1	75	1.1		6.3–6.9	76

[a] $abdc^{2-}$ = 4,4′-azobenzenedicarboxylate; $abtc^{4-}$ = azobenzene-3,3′,5,5′-tetracarboxylate; adc^{2-} = 9,10-anthracenedicarboxylate; $aobtc^{4-}$ = azoxybenzene-3,3′,5,5′-tetracarboxylate; atc = 3,5-dicarboxyl-(3′,5′-dicarboxylazophenyl)benzene; bdc^{2-} = 1,4-benzenedicarboxylate; BDP^{2-} = 1,4-benzenedipyrazolate; BDT^{2-} = 1,4-benzenebistetrazolate; $bhtc^{3-}$ = biphenyl-3,4′,5-tricarboxylate; $bpdc^{2-}$ = 4,4′-biphenyldicarboxylate; bpe = 4,4′-*trans*-bis(4-pyridyl)-ethylene; $bpndc^{2-}$ = benzophenone-4,4′-dicarboxylate; $bptc^{4-}$ = 3,3′,5,5′-biphenyltetracarboxylate; bpy = 4,4′-bipyridine; $bpydc^{2-}$ = 2,2′-bipyridyl-5,5′-dicarboxylate; $bpytc^{4-}$ = 4,4′-bipyridine-2,6,2′,6′-tetracarboxylate; $Brbdc^{2-}$ = 2-bromobenzene-1,4-dicarboxylate; $btatb^{4-}$ = 4,4′,4″,4‴-benzene-1,2,4,5-tetrayltetrabenzoate; H_3BTB = 1,3,5-tri(4-carboxyphenyl)benzene; BTT^{3-} = 1,3,5-benzenetristetrazolate; H_2cdc = 1,12-dihydroxycarbonyl-1,12-dicarba-*closo*-dodecaborane; CF_3Py = 4-(α,α,α-trifluoromethyl)pyridine; H_2cnc = 4-carboxycinnamic acid; dabco = 1,4-diazabicyclo[2.2.2]octane; $dbdc^{2-}$ = 1,2-dihydrocyclobutabenzene-3,6-dicarboxylate; $dcctp^{-}$ = 3,5-dicyano-4-(4-carboxyphenyl)-2,2′:6′,4″-terpyridine; $dcdBn^{2-}$ = 6,6′-dichloro-2,2′-dibenzyloxy-1,1′-binaphthyl-4,4′-dibenzoate; $dcdEt^{2-}$ = 6,6′-dichloro-2,2′-diethoxy-1,1′-binaphthyl-4,4′-dibenzoate; H_4dhtp = 2,5-dihydroxyterephthalic acid; diPyNI = *N*,*N*′-di(4-pyridyl)-1,4,5,8-naphthalenetetracarboxydiimide; DMF = *N*,*N*′-dimethylformamide; dpac = 4,4′-dipyridylacetylene; dpt = 3,6-di(4-pyridyl)-1,2,4,5-tetrazine; EtPy = 4-ethylpyridine; $F\text{-}pymo^{-}$ = 5-fluoropyrimidin-2-olate; fum^{2-} = fumarate; $H_2hfipbb$ = 4,4-(hexafluoroisopropylidene)bis(benzoic acid); H_2Nbdc = 2-aminobenzene-1,4-dicarboxylate; $hfipbb^{2-}$ = 4,4-(hexafluoroisopropylidene)bis(benzoate); $hpdc^{2-}$ = 4,5,9,10-tetrahydropyrene-2,7-dicarboxylate; $mdip^{4-}$ = 5,5′-methylene diisophthalate; $MeIM^{-}$ = 2-methylimidazole; MePy = 4-methylpyridine; mna^{2-} = 6-mercaptonicotinate; NDC^{2-} = 2,6-naphthalenedicarboxylate; $1,4\text{-}ndc^{2-}$ = 1,4-naphthalenedicarboxylate; ntb^{3-} = 4,4′,4″-nitrilotrisbenzoate; ntc^{4-} = naphthalene-1,4,5,8-tetracarboxylate; ox^{2-} = oxalate; $oxdc^{2-}$ = oxydiacetate; $pbpc^{2-}$ = pyridine-3,5-bis(phenyl-4-carboxylate); pda^{2-} = *p*-phenylenediacrylate; $2,4\text{-}pdc^{2-}$ = 2,4-pyridinedicarboxylate; $3,5\text{-}pdc^{2-}$ = 3,5-pyridinedicarboxylate; $PhIm^{-}$ = 2-phenylimidazole; pyen = conjugate base of 5-methyl-4-oxo-1,4-dihydro-pyridine-3-carbaldehyde; $pymc^{-}$ = 2-pyrimidinecarboxylate; $pymdc^{2-}$ = 3,5-pyrimidinedicarboxylate; $2\text{-}pymo^{-}$ = 2-pyrimidinolate; $4\text{-}pymo^{-}$ = 4-pyrimidinolate; $pyrdc^{2-}$ = pyrene-2,7-dicarboxylate; pyz = pyrazine; $qptc^{4-}$ = quaterphenyl-3,3‴,5,5‴-tetracarboxylate; $sbtc^{4-}$ = *trans*-stilbene-3,3′,5,5′-tetracarboxylic acid; sip^{3-} = 5-sulfoisophthalate; $tatb^{3-}$ = 4,4′,4″-*s*-triazine-2,4,6-triyltribenzoate; $tbip^{2-}$ = 5-*t*-butyl isophthalate; $H_4tcpcdp$ = 3,3′,5,5′-tetra(4-carboxyphenyl)-2,2′-diethoxylbiphenyl; $H_4tcpdep$ = 3,3′,5,5′-tetra(4-carboxyphenyl)-2,2′-diethoxylbiphenyl; $H_4(C_{2h}\text{-}tcppda)$ = *meso* diastereomer of *N*,*N*,*N*′,*N*′-tetrakis(4-carboxyphenyl)-1,4-phenylenediamine; $H_4(D_2\text{-}tcppda)$ = δ and λ enantiomers for the *D* diastereomer of *N*,*N*,*N*′,*N*′-tetrakis(4-carboxyphenyl)-1,4-phenylenediamine; $tfbdc^{2-}$ = tetrafluoroterephthalate; $tmbdc^{2-}$ = tetramethylterephthalate; $tptc^{4-}$ = terphenyl-3,3″,5,5″-tetracarboxylate; $H_3tpb\text{-}3tz$ = 1,3,5-tri-*p*-(tetrazol-5-yl)phenylbenzene; $H_3tpt\text{-}3tz$ = 2,4,6-tri-*p*-(tetrazol-5-yl)phenyl-*s*-triazine; trz^{-} = 1,2,4-triazolate; $ttdc^{2-}$ = thieno[3,2-*b*]thiophene-2,5-dicarboxylate; $ttpm^{4-}$ = tetrakis(4-tetrazolylphenyl)methane; tzi^{2-} = 5-tetrazolylisophthalate; ViPy = 4-vinylpyridine. [b] Values in parentheses are total uptake. [c] Irreversible. [d] Measured using carbon dioxide. [e] Measured in mL (H_2 at STP) mL^{-1}. [f] Measured with methanol.

References

1 Energy Information Administration, Official Energy Statistics from the U.S. Government, International Energy Annual 2005, available at: http://www.eia.doe.gov/emeu/iea/.
2 U.S. Department of Transportation, Federal Highway Administration, Our Nation's Highways—2000, available at: http://www.fhwa.dot.gov/ohim/onh00/.
3 A. W. C. van den Berg and C. Otero Areán, *Chem. Commun.*, 2008, 668–681.
4 DoE Office of Energy Efficiency and Renewable Energy Hydrogen, Fuel Cells & Infrastructure Technologies Program, 'Grand Challenge' for Basic and Applied Research in Hydrogen Storage Solicitation, available at: http://www.eere.energy.gov/hydrogenandfuelcells/2003_storage_solicitation.html.
5 DoE Office of Energy Efficiency and Renewable Energy Hydrogen, Fuel Cells & Infrastructure Technologies Program Multi-Year Research, Development and Demonstration Plan, available at: http://www.eere.energy.gov/hydrogenandfuelcells/mypp.
6 R. C. Lochan and M. Head-Gordon, *Phys. Chem. Chem. Phys.*, 2006, **8**, 1357–1370.
7 T. Düren and R. Q. Snurr, *J. Phys. Chem. B*, 2004, **108**, 15703–15708.
8 H. Frost, T. Düren and R. Q. Snurr, *J. Phys. Chem. B*, 2006, **110**, 9565–9570.
9 H. Frost and R. Q. Snurr, *J. Phys. Chem. C*, 2007, **111**, 18794–18803.
10 E. Klontzas, A. Mavrandonakis, G. E. Froudakis, Y. Carissan and W. Klopper, *J. Phys. Chem. C*, 2007, **111**, 13635–13640.
11 E. Klontzas, A. Mavrandonakis, E. Tylianakis and G. E. Froudakis, *Nano Lett.*, 2008, **8**, 1572–1576.
12 E. Klontzas, E. Tylianakis and G. E. Froudakis, *J. Phys. Chem. C*, 2008, **112**, 9095–9098.
13 A. Mavrandonakis, E. Tylianakis, A. K. Stubos and G. E. Froudakis, *J. Phys. Chem. C*, 2008, **112**, 7290–7294.
14 S. S. Han, W.-Q. Deng and W. A. Goddard III, *Angew. Chem., Int. Ed.*, 2007, **46**, 6289–6292.
15 S. S. Han, H. Furukawa, O. M. Yaghi and I. W. A. Goddard, *J. Am. Chem. Soc.*, 2008, **130**, 11580–11581.
16 S. S. Han and W. A. Goddard III, *J. Phys. Chem. C*, 2007, **111**, 15185–15191.
17 S. S. Han and W. A. Goddard III, *J. Am. Chem. Soc.*, 2007, **129**, 8422–8423.
18 J. L. Belof, A. C. Stern and B. Space, *J. Chem. Theory Comput.*, 2008, **4**, 1332–1337.
19 S. S. Kaye, A. Dailly, O. M. Yaghi and J. R. Long, *J. Am. Chem. Soc.*, 2007, **129**, 14176–14177.
20 R. C. Lochan, R. Z. Khaliullin and M. Head-Gordon, *Inorg. Chem.*, 2008, **47**, 4032–4044.
21 M. Dincă, A. Dailly, Y. Liu, C. M. Brown, D. A. Neumann and J. R. Long, *J. Am. Chem. Soc.*, 2006, **128**, 16876–16883.
22 Y. Y. Sun, Y.-H. Kim and S. B. Zhang, *J. Am. Chem. Soc.*, 2007, **129**, 12606–12607.
23 W. Zhou and T. Yildirim, *J. Phys. Chem. C*, 2008, **112**, 8132–8135.
24 S. K. Bhatia and A. L. Myers, *Langmuir*, 2006, **22**, 1688–1700.
25 E. Garrone, B. Bonelli and C. Otero Areán, *Chem. Phys. Lett.*, 2008, **456**, 68–70.
26 M. Rzepka, P. Lamp and M. A. de la Casa-Lillo, *J. Phys. Chem. B*, 1998, **102**, 10894–10898.
27 M. Dincă, W. S. Han, Y. Liu, A. Dailly, C. M. Brown and J. R. Long, *Angew. Chem., Int. Ed.*, 2007, **45**, 1419–1422.
28 M. Dincă and J. R. Long, *J. Am. Chem. Soc.*, 2007, **129**, 11172–11176.
29 K. S. Park, Z. Ni, A. P. Côté, J. Y. Choi, R. Huang, F. J. Uribe-Romo, H. K. Chae, M. O'Keeffe and O. M. Yaghi, *Proc. Natl. Acad. Sci. U. S. A.*, 2006, **103**, 10186–10191.
30 H. Wu, W. Zhou and T. Yildirim, *J. Am. Chem. Soc.*, 2007, **129**, 5314–5315.
31 W. Zhou, H. Wu, M. R. Hartman and T. Yildirim, *J. Phys. Chem. C*, 2007, **111**, 16131–16137.
32 H. Park, J. F. Britten, U. Mueller, J. Y. Lee, J. Li and J. B. Parise, *Chem. Mater.*, 2007, **19**, 1302–1308.
33 H. Park, G. Krigsfeld and J. B. Parise, *Cryst. Growth Des.*, 2007, **7**, 736–740.
34 X.-L. Wang, C. Qin, E.-B. Wang and Z.-M. Su, *Chem.–Eur. J.*, 2006, **12**, 2680–2691.
35 C. Yang, X. Wang and M. A. Omary, *J. Am. Chem. Soc.*, 2007, **129**, 15454–15455.
36 Q.-G. Zhai, C.-Z. Lu, X.-Y. Wu and S. R. Batten, *Cryst. Growth Des.*, 2007, **7**, 2332–2342.
37 H. J. Choi, M. Dincă and J. R. Long, *J. Am. Chem. Soc.*, 2008, **130**, 7848–7850.
38 G. J. Kubas, *Metal Dihydrogen and σ-Bond Complexes—Structure, Theory, and Reactivity*, Kluwer Academic, New York, Boston, Dordrecht, London, Moscow, 2001.
39 C. H. Wu, *J. Chem. Phys.*, 1979, **71**, 783–787.
40 S. S. Kaye and J. R. Long, *Chem. Commun.*, 2007, 4486–4488.
41 M. Dincă and J. R. Long, *Angew. Chem., Int. Ed.*, 2008, **47**, 6766–6779.
42 C. Prestipino, L. Regli, J. G. Vitillo, F. Bonino, A. Damin, C. Lamberti, A. Zecchina, P. L. Solari, K. O. Kongshaug and S. Bordiga, *Chem. Mater.*, 2006, **18**, 1337–1346.
43 S. S. Kaye and J. R. Long, *J. Am. Chem. Soc.*, 2008, **130**, 806–807.
44 S. S. Kaye and J. R. Long, *J. Am. Chem. Soc.*, 2005, **127**, 6506–6507.
45 K. L. Mulfort and J. T. Hupp, *J. Am. Chem. Soc.*, 2007, **129**, 9604–9605.
46 J. L. Belof, A. C. Stern, M. Eddaoudi and B. Space, *J. Am. Chem. Soc.*, 2007, **129**, 15202–15210.
47 H. Kabbour, T. F. Baumann, J. H. Satcher, A. Saulnier and C. C. Ahn, *Chem. Mater.*, 2006, **18**, 6085–6087.
48 D. Sun, S. Ma, Y. Ke, D. J. Collins and H.-C. Zhou, *J. Am. Chem. Soc.*, 2006, **128**, 3896–3897.
49 S. Ma, D. Sun, M. Ambrogio, J. A. Fillinger, S. Parkin and H.-C. Zhou, *J. Am. Chem. Soc.*, 2007, **129**, 1858–1859.
50 M. Dincă, A. Dailly, C. Tsay and J. R. Long, *Inorg. Chem.*, 2008, **47**, 11–13.
51 G. A. Somorjai, *Surf. Sci.*, 1994, **299–300**, 849–866.
52 K. Christmann, G. Ertl and T. Pignet, *Surf. Sci.*, 1976, **54**, 365–392.
53 R. A. Olsen, G. J. Kroes and E. J. Baerends, *J. Chem. Phys.*, 1999, **111**, 11155–11163.
54 A. T. Pasteur, S. J. Dixon-Warren, Q. Ge and D. A. King, *J. Chem. Phys.*, 1997, **106**, 8896–8904.
55 A. T. Gee, B. E. Hayden, C. Mormiche and T. S. Nunney, *J. Chem. Phys.*, 2000, **112**, 7660–7668.
56 S. Khoobiar, *J. Phys. Chem.*, 1964, **68**, 411–412.
57 L. Wang and R. T. Yang, *Energy Environ. Sci.*, 2008, **1**, 268–279.
58 H. Cheng, L. Chen, A. C. Cooper, X. Sha and G. P. Pez, *Energy Environ. Sci.*, 2008, **1**, 338–354.
59 Y. Li, F. H. Yang and R. T. Yang, *J. Phys. Chem. C*, 2007, **111**, 3405–3411.
60 Y. Li and R. T. Yang, *J. Am. Chem. Soc.*, 2006, **128**, 726–727.
61 Y. Li and R. T. Yang, *J. Am. Chem. Soc.*, 2006, **128**, 8136–8137.
62 Y. Li and R. T. Yang, *Langmuir*, 2007, **23**, 12937–12944.
63 Y. Li and R. T. Yang, *AIChE J.*, 2008, **54**, 269–279.
64 Y.-Y. Liu, J.-L. Zeng, J. Zhang, F. Xu and L.-X. Sun, *Int. J. Hydrogen Energy*, 2007, **32**, 4005–4010.
65 N. L. Rosi, J. Eckert, M. Eddaoudi, D. T. Vodak, J. Kim, M. O'Keeffe and O. M. Yaghi, *Science*, 2003, **300**, 1127–1129.
66 J. L. C. Rowsell, A. R. Millward, K. S. Park and O. M. Yaghi, *J. Am. Chem. Soc.*, 2004, **126**, 5666–5667.
67 B. Panella, M. Hirscher, H. Pütter and U. Müller, *Adv. Funct. Mater.*, 2006, **16**, 520–524.
68 L. Pan, M. B. Sander, X. Huang, J. Li, M. R. Smith, E. W. Bittner, B. C. Bockrath and J. K. Johnson, *J. Am. Chem. Soc.*, 2004, **126**, 1308–1309.
69 A. G. Wong-Foy, A. J. Matzger and O. M. Yaghi, *J. Am. Chem. Soc.*, 2006, **128**, 3494–3495.
70 B. Panella and M. Hirscher, *Adv. Mater.*, 2005, **17**, 538–541.
71 M. Sabo, A. Henschel, H. Fröde, E. Klemm and S. Kaskel, *J. Mater. Chem.*, 2007, **17**, 3827–3832.
72 D. N. Dybtsev, H. Chun and K. Kim, *Angew. Chem., Int. Ed.*, 2004, **43**, 5033–5036.
73 J. Y. Lee, D. H. Olson, L. Pan, T. J. Emge and J. Li, *Adv. Funct. Mater.*, 2007, **17**, 1255–1262.
74 J. Liu, J. Y. Lee, L. Pan, R. T. Obermyer, S. Simizu, B. Zande, J. Li, S. G. Sankar and J. K. Johnson, *J. Phys. Chem. C*, 2008, **112**, 2911–2917.

75 J. Hafizovic, M. Bjrgen, U. Olsbye, P. D. C. Dietzel, S. Bordiga, C. Prestipino, C. Lamberti and K. P. Lillerud, *J. Am. Chem. Soc.*, 2007, **129**, 3612–3620.
76 S. S. Kaye and J. R. Long, *Catal. Today*, 2007, **120**, 311–316.
77 D. Zhao, D. Yuan and H.-C. Zhou, *Energy Environ. Sci.*, 2008, **1**, 222–235.
78 H. Furukawa, M. A. Miller and O. M. Yaghi, *J. Mater. Chem.*, 2007, **17**, 3197–3204.
79 B. A. Younglove, *J. Phys. Chem. Ref. Data*, 1982, **11**, 1.
80 E. C. Spencer, J. A. K. Howard, G. J. McIntyre, J. L. C. Rowsell and O. M. Yaghi, *Chem. Commun.*, 2006, 278–280.
81 B. Chen, X. Zhao, A. Putkham, K. Hong, E. B. Lobkovsky, E. J. Hurtado, A. J. Fletcher and K. M. Thomas, *J. Am. Chem. Soc.*, 2008, **130**, 6411–6423.
82 S. Bordiga, L. Regli, F. Bonino, E. Groppo, C. Lamberti, B. Xiao, P. S. Wheatley, J. J. Morris and A. Zecchina, *Phys. Chem. Chem. Phys.*, 2007, **9**, 2676–2685.
83 R. C. Mehrotra and R. Bohra, *Metal Carboxylates*, Academic Press, London, New York, 1983.
84 I. Senkovska and S. Kaskel, *Eur. J. Inorg. Chem.*, 2006, **2006**, 4564–4569.
85 G. Férey, M. Latroche, C. Serre, F. Millange, T. Loiseau and A. Percheron-Guégan, *Chem. Commun.*, 2003, 2976–2977.
86 M. Latroche, S. Surblé, C. Serre, C. Mellot-Draznieks, P. L. Llewellyn, J.-H. Lee, J.-S. Chang, S. H. Jhung and G. Férey, *Angew. Chem., Int. Ed.*, 2006, **45**, 8227–8231.
87 X. Lin, J. Jia, X. Zhao, K. M. Thomas, A. J. Blake, G. S. Walker, N. R. Champness, P. Hubberstey and M. Schröder, *Angew. Chem., Int. Ed.*, 2006, **45**, 7358–7364.
88 V. K. Peterson, Y. Liu, C. M. Brown and C. J. Kepert, *J. Am. Chem. Soc.*, 2006, **128**, 15578–15579.
89 X.-S. Wang, S. Ma, P. M. Forster, D. Yuan, J. Eckert, J. J. López, B. J. Murphy, J. B. Parise and H.-C. Zhou, *Angew. Chem., Int. Ed.*, 2008, **47**, 7263–7266.
90 P. D. C. Dietzel, Y. Morita, R. Blom and H. Fjellvåg, *Angew. Chem., Int. Ed.*, 2005, **44**, 6354–6358.
91 P. D. C. Dietzel, B. Panella, M. Hirscher, R. Blom and H. Fjellvåg, *Chem. Commun.*, 2006, 959–961.
92 S. R. Caskey, A. G. Wong-Foy and A. J. Matzger, *J. Am. Chem. Soc.*, 2008, **130**, 10870–10871.
93 N. L. Rosi, J. Kim, M. Eddaoudi, B. Chen, M. O' Keeffe and O. M. Yaghi, *J. Am. Chem. Soc.*, 2005, **127**, 1504–1518.
94 W. Zhou, H. Wu and T. Yildirim, *J. Am. Chem. Soc.*, 2008, **130**, 15268–15269.
95 H. Chun, D. Kim, D. N. Dybtsev and K. Kim, *Angew. Chem., Int. Ed.*, 2004, **116**, 989–992.
96 M. Dincă, A. F. Yu and J. R. Long, *J. Am. Chem. Soc.*, 2006, **128**, 8904–8913.
97 J. Catalán and J. Elguero, *J. Chem. Soc., Perkin Trans. 2*, 1983, 1869–1874.
98 X. Zhao, B. Xiao, A. J. Fletcher, K. M. Thomas, D. Bradshaw and M. J. Rosseinsky, *Science*, 2004, **306**, 1012–1015.
99 T. A. Strobel, C. J. Taylor, K. C. Hester, S. F. Dec, C. A. Koh, K. T. Miller and E. D. Sloan, *J. Phys. Chem. B*, 2006, **110**, 17121–17125.
100 L. J. Florusse, C. J. Peters, J. Schoonman, K. C. Hester, C. A. Koh, S. F. Dec, K. N. Marsh and E. D. Sloan, *Science*, 2004, **306**, 469–471.
101 W. L. Mao, H.-k. Mao, A. F. Goncharov, V. V. Struzhkin, Q. Guo, J. Hu, J. Shu, R. J. Hemley, M. Somayazulu and Y. Zhao, *Science*, 2002, **297**, 2247–2249.
102 F. Nouar, J. F. Eubank, T. Bousquet, L. Wojtas, M. J. Zaworotko and M. Eddaoudi, *J. Am. Chem. Soc.*, 2008, **130**, 1833–1835.
103 L. Reguera, J. Balmaseda, L. F. d. Castillo and E. Reguera, *J. Phys. Chem. C*, 2008, **112**, 5589–5597.
104 H. M. El-Kaderi, J. R. Hunt, J. L. Mendoza-Cortes, A. P. Cote, R. E. Taylor, M. O'Keeffe and O. M. Yaghi, *Science*, 2007, **316**, 268–272.
105 Y. Zhang, L. G. Scanlon, M. A. Rottmayer and P. B. Balbuena, *J. Phys. Chem. B*, 2006, **110**, 22532–22541.
106 Y. J. Choi, J. W. Lee, J. H. Choi and J. K. Kang, *Appl. Phys. Lett.*, 2008, **92**, 173102–173103.
107 T. Yildirim and M. R. Hartman, *Phys. Rev. Lett.*, 2005, **95**, 215504.
108 F. M. Mulder, T. J. Dingemans, M. Wagemaker and G. J. Kearley, *Chem. Phys.*, 2005, **317**, 113–118.
109 F. M. Mulder, T. J. Dingemans, H. G. Schimmel, A. J. Ramirez-Cuesta and G. J. Kearle, *J. Chem. Phys.*, 2008, **351**, 72–76.
110 J. L. C. Rowsell, J. Eckert and O. M. Yaghi, *J. Am. Chem. Soc.*, 2005, **127**, 14904–14910.
111 Y. Liu, H. Kabbour, C. M. Brown, D. A. Neumann and C. C. Ahn, *Langmuir*, 2008, **24**, 4772–4777.
112 Y. Liu, C. M. Brown, D. A. Neumann, V. K. Peterson and C. J. Kepert, *J. Alloys Compd.*, 2007, **446–447**, 385–388.
113 J. Luo, H. Xu, Y. Liu, Y. Zhao, L. L. Daemen, C. M. Brown, T. V. Timofeeva, S. Ma and H.-C. Zhou, *J. Am. Chem. Soc.*, 2008, **130**, 9626–9627.
114 M. R. Hartman, V. K. Peterson, Y. Liu, S. S. Kaye and J. R. Long, *Chem. Mater.*, 2006, **18**, 3221–3224.
115 K. W. Chapman, P. J. Chupas, E. R. Maxey and J. W. Richardson, *Chem. Commun.*, 2006, 4013–4015.
116 P. M. Forster, J. Eckert, B. D. Heiken, J. B. Parise, J. W. Yoon, S. H. Jhung, J.-S. Chang and A. K. Cheetham, *J. Am. Chem. Soc.*, 2006, **128**, 16846–16850.
117 A. Zecchina, C. Otero Areán, G. Turnes Palomino, F. Geobaldo, C. Lamberti, G. Spoto and S. Bordiga, *Phys. Chem. Chem. Phys.*, 1999, **1**, 1649–1657.
118 E. Groppo, C. Lamberti, S. Bordiga, G. Spoto, A. Damin and A. Zecchina, *J. Phys. Chem. B*, 2005, **109**, 15024–15031.
119 S. Bordiga, J. G. Vitillo, G. Ricchiardi, L. Regli, D. Cocina, A. Zecchina, B. Arstad, M. Bjrgen, J. Hafizovic and K. P. Lillerud, *J. Phys. Chem. B*, 2005, **109**, 18237–18242.
120 J. G. Vitillo, L. Regli, S. Chavan, G. Ricchiardi, G. Spoto, P. D. C. Dietzel, S. Bordiga and A. Zecchina, *J. Am. Chem. Soc.*, 2008, **130**, 8386–8396.
121 J. Y. Lee, J. Li and J. Jagiello, *J. Solid State Chem.*, 2005, **178**, 2527–2532.
122 J. L. C. Rowsell and O. M. Yaghi, *J. Am. Chem. Soc.*, 2006, **128**, 1304–1315.
123 J. A. Rood, B. C. Noll and K. W. Henderson, *Inorg. Chem.*, 2006, **45**, 5521–5528.
124 M. Dincă and J. R. Long, *J. Am. Chem. Soc.*, 2005, **127**, 9376–9377.
125 T. Loiseau, L. Lecroq, C. Volkringer, J. Marrot, G. Férey, M. Haouas, F. Taulelle, S. Bourrelly, P. L. Llewellyn and M. Latroche, *J. Am. Chem. Soc.*, 2006, **128**, 10223–10230.
126 J. Perles, M. Iglesias, M.-Á. Martín-Luengo, M. Á. Monge, C. Ruiz-Valero and N. Snejko, *Chem. Mater.*, 2005, **17**, 5837–5842.
127 S. Surblé, F. Millange, C. Serre, T. Düren, M. Latroche, S. Bourrelly, P. L. Llewellyn and G. Férey, *J. Am. Chem. Soc.*, 2006, **128**, 14889–14896.
128 D. N. Dybtsev, H. Chun, S. H. Yoon, D. Kim and K. Kim, *J. Am. Chem. Soc.*, 2004, **126**, 32–33.
129 H. R. Moon, N. Kobayashi and M. P. Suh, *Inorg. Chem.*, 2006, **45**, 8672–8676.
130 J. Jia, X. Lin, C. Wilson, A. J. Blake, N. R. Champness, P. Hubberstey, G. Walker, E. J. Cussen and M. Schröder, *Chem. Commun.*, 2007, 840–842.
131 J. H. Yoon, S. B. Choi, Y. J. Oh, M. J. Seo, Y. H. Jhon, T.-B. Lee, D. Kim, S.-H. Choi and J. Kim, *Catal. Today*, 2007, **120**, 324–329.
132 S. B. Choi, M. J. Seo, M. Cho, Y. Kim, M. K. Jin, D.-Y. Jung, J.-S. Choi, W.-S. Ahn, J. L. C. Rowsell and J. Kim, *Cryst. Growth Des.*, 2007, **7**, 2290–2293.
133 Y. Li, L. Xie, Y. Liu, R. Yang and X. Li, *Inorg. Chem.*, 2008, **47**, 10372–10377.
134 B. Chen, S. Ma, E. J. Hurtado, E. B. Lobkovsky, C. Liang, H. Zhu and S. Dai, *Inorg. Chem.*, 2007, **46**, 8705–8709.
135 S. M. Humphrey, J.-S. Chang, S. H. Jhung, J. W. Yoon and P. T. Wood, *Angew. Chem., Int. Ed.*, 2007, **46**, 272–275.
136 L.-G. Zhu and H.-P. Xiao, *Z. Anorg. Allg. Chem.*, 2008, **634**, 845–847.
137 T. Takei, J. Kawashima, T. Ii, A. Maeda, M. Hasegawa, T. Kitagawa, T. Ohmura, M. Ichikawa, M. Hosoe, I. Kanoya and W. Mori, *Bull. Chem. Soc. Jpn.*, 2008, **81**, 847–856.
138 H. Chun, H. Jung, G. Koo, H. Jeong and D.-K. Kim, *Inorg. Chem.*, 2008, **47**, 5355–5359.
139 J. Y. Lee, L. Pan, S. P. Kelly, J. Jagiello, T. J. Emge and J. Li, *Adv. Mater.*, 2005, **17**, 2703–2706.

140 S. Ma and H.-C. Zhou, *J. Am. Chem. Soc.*, 2006, **128**, 11734–11735.
141 E. Y. Lee and M. P. Suh, *Angew. Chem., Int. Ed.*, 2004, **43**, 2798–2801.
142 P. D. C. Dietzel, B. Panella, M. Hirscher, R. Blom and H. Fjellvåg, *Chem. Commun.*, 2006, 959–961.
143 A. J. Cairns, J. A. Perman, L. Wojtas, V. C. Kravtsov, M. H. Alkordi, M. Eddaoudi and M. J. Zaworotko, *J. Am. Chem. Soc.*, 2008, **130**, 1560–1561.
144 S. Ma, X.-S. Wang, E. S. Manis, C. D. Collier and H.-C. Zhou, *Inorg. Chem.*, 2007, **46**, 3432–3434.
145 D. Noguchi, H. Tanaka, A. Kondo, H. Kajiro, H. Noguchi, T. Ohba, H. Kanoh and K. Kaneko, *J. Am. Chem. Soc.*, 2008, **130**, 6367–6372.
146 W. Yang, X. Lin, J. Jia, A. J. Blake, C. Wilson, P. Hubberstey, N. R. Champness and M. Schröder, *Chem. Commun.*, 2008, 359–361.
147 B. Chen, S. Ma, F. Zapata, F. R. Fronczek, E. B. Lobkovsky and H.-C. Zhou, *Inorg. Chem.*, 2007, **46**, 1233–1236.
148 J. A. R. Navarro, E. Barea, J. M. Salas, N. Masciocchi, S. Galli, A. Sironi, C. O. Ania and J. B. Parra, *Inorg. Chem.*, 2006, **45**, 2397–2399.
149 J. A. R. Navarro, E. Barea, A. Rodríguez-Diéguez, J. M. Salas, C. O. Ania, J. B. Parra, N. Masciocchi, S. Galli and A. Sironi, *J. Am. Chem. Soc.*, 2008, **130**, 3978–3984.
150 D. Sun, Y. Ke, T. M. Mattox, B. A. Ooro and H.-C. Zhou, *Chem. Commun.*, 2005, 5447–5449.
151 L. Ma, J. Y. Lee, J. Li and W. Lin, *Inorg. Chem.*, 2008, **47**, 3955–3957.
152 M. Xue, G. Zhu, Y. Li, X. Zhao, Z. Jin, E. Kang and S. Qiu, *Cryst. Growth Des.*, 2008, **8**, 2478–2483.
153 Y.-G. Lee, H. R. Moon, Y. E. Cheon and M. P. Suh, *Angew. Chem., Int. Ed.*, 2008, **47**, 7741–7745.
154 X.-S. Wang, S. Ma, K. Rauch, J. M. Simmons, D. Yuan, X. Wang, T. Yildirim, W. C. Cole, J. J. López, A. de Meijere and H.-C. Zhou, *Chem. Mater.*, 2008, **20**, 3145–3152.
155 H. J. Park and M. P. Suh, *Chem.–Eur. J.*, 2008, **14**, 8812–8821.
156 B. Chen, N. W. Ockwig, A. R. Millward, D. S. Contreras and O. M. Yaghi, *Angew. Chem., Int. Ed.*, 2005, **44**, 4745–4749.
157 A. G. Wong-Foy, O. Lebel and A. J. Matzger, *J. Am. Chem. Soc.*, 2007, **129**, 15740–15741.
158 P. Krawiec, M. Kramer, M. Sabo, R. Kunschke, H. Fröde and S. Kaskel, *Adv. Eng. Mater.*, 2006, **8**, 293–296.
159 B. Xiao, P. S. Wheatley, X. Zhao, A. J. Fletcher, S. Fox, A. G. Rossi, I. L. Megson, S. Bordiga, L. Regli, K. M. Thomas and R. E. Morris, *J. Am. Chem. Soc.*, 2007, **129**, 1203–1209.
160 B. Chen, S. Ma, E. J. Hurtado, E. B. Lobkovsky and H.-C. Zhou, *Inorg. Chem.*, 2007, **46**, 8490–8492.
161 B. Chen, C. Liang, J. Yang, D. S. Contreras, Y. L. Clancy, E. B. Lobkovsky, O. M. Yaghi and S. Dai, *Angew. Chem., Int. Ed.*, 2006, **45**, 1390–1393.
162 B. Chen, S. Ma, F. Zapata, E. B. Lobkovsky and J. Yang, *Inorg. Chem.*, 2006, **45**, 5718–5720.
163 L. Pan, B. Parker, X. Huang, D. H. Olson, J. Y. Lee and J. Li, *J. Am. Chem. Soc.*, 2006, **128**, 4180–4181.
164 H. Chun, D. N. Dybtsev, H. Kim and K. Kim, *Chem.–Eur. J.*, 2005, **11**, 3521–3529.
165 X. Lin, A. J. Blake, C. Wilson, X. Z. Sun, N. R. Champness, M. W. George, P. Hubberstey, R. Mokaya and M. Schröder, *J. Am. Chem. Soc.*, 2006, **128**, 10745–10753.
166 O. K. Farha, K. L. Mulfort and J. T. Hupp, *Inorg. Chem.*, 2008, **47**, 10223–10225.
167 M. Xue, S. Ma, Z. Jin, R. M. Schaffino, G.-S. Zhu, E. B. Lobkovsky, S.-L. Qiu and B. Chen, *Inorg. Chem.*, 2008, **47**, 6825–6828.
168 O. K. Farha, A. M. Spokoyny, K. L. Mulfort, M. F. Hawthorne, C. A. Mirkin and J. T. Hupp, *J. Am. Chem. Soc.*, 2007, **129**, 12680–12681.
169 D. Sun, Y. Ke, D. J. Collins, G. A. Lorigan and H.-C. Zhou, *Inorg. Chem.*, 2007, **46**, 2725–2734.
170 S. Ma, X.-S. Wang, C. D. Collier, E. S. Manis and H.-C. Zhou, *Inorg. Chem.*, 2007, **46**, 8499–8501.
171 A. Dailly, J. J. Vajo and C. C. Ahn, *J. Phys. Chem. B*, 2006, **110**, 1099–1101.
172 D. Sun, D. J. Collins, Y. Ke, J.-L. Zuo and H.-C. Zhou, *Chem.–Eur. J.*, 2006, **12**, 3768–3776.
173 B. Kesanli, Y. Cui, M. R. Smith, E. W. Bittner, B. C. Bockrath and W. Lin, *Angew. Chem., Int. Ed.*, 2005, **44**, 72–75.
174 E. Y. Lee, S. Y. Jang and M. P. Suh, *J. Am. Chem. Soc.*, 2005, **127**, 6374–6381.
175 Q.-R. Fang, G.-S. Zhu, M. Xue, Q.-L. Zhang, J.-Y. Sun, X.-D. Guo, S.-L. Qiu, S.-T. Xu, P. Wang, D.-J. Wang and Y. Wei, *Chem.–Eur. J.*, 2006, **12**, 3754–3758.
176 J. Jia, X. Lin, A. J. Blake, N. R. Champness, P. Hubberstey, L. Shao, G. S. Walker, C. Wilson and M. Schröder, *Inorg. Chem.*, 2006, **45**, 8838–8840.
177 M. Kramer, U. Schwarz and S. Kaskel, *J. Mater. Chem.*, 2006, **16**, 2245–2248.
178 J. A. R. Navarro, E. Barea, J. M. Salas, N. Masciocchi, S. Galli, A. Sironi, C. O. Ania and J. B. Parra, *J. Mater. Chem.*, 2007, **17**, 1939–1946.
179 D. F. Sava, V. C. Kravtsov, F. Nouar, L. Wojtas, J. F. Eubank and M. Eddaoudi, *J. Am. Chem. Soc.*, 2008, **130**, 3768–3770.
180 Q.-R. Fang, G.-S. Zhu, Z. Jin, Y.-Y. Ji, J.-W. Ye, M. Xue, H. Yang, Y. Wang and S.-L. Qiu, *Angew. Chem., Int. Ed.*, 2007, **46**, 6638–6642.
181 Y. Liu, J. F. Eubank, A. J. Cairns, J. Eckert, V. C. Kravtsov, R. Luebke and M. Eddaoudi, *Angew. Chem., Int. Ed.*, 2007, **46**, 3278–3283.
182 Y. Wang, P. Cheng, J. Chen, D.-Z. Liao and S.-P. Yan, *Inorg. Chem.*, 2007, **46**, 4530–4534.
183 X. Guo, G. Zhu, Z. Li, F. Sun, Z. Yang and S. Qiu, *Chem. Commun.*, 2006, 3172–3174.
184 S. Ma, X.-S. Wang, D. Yuan and H.-C. Zhou, *Angew. Chem., Int. Ed.*, 2008, **47**, 4130–4133.
185 L. Reguera, C. P. Krap, J. Balmaseda and E. Reguera, *J. Phys. Chem. C*, 2008, **112**, 15893–15899.
186 J. T. Culp, S. Natesakhawat, M. R. Smith, E. Bittner, C. Matranga and B. Bockrath, *J. Phys. Chem. C*, 2008, **112**, 7079–7083.
187 J. T. Culp, C. Matranga, M. Smith, E. W. Bittner and B. Bockrath, *J. Phys. Chem. B*, 2006, **110**, 8325–8328.
188 L. Reguera, J. Balmaseda, C. P. Krap, M. Avila and E. Reguera, *J. Phys. Chem. C*, 2008, **112**, 17443–17449.

